12-11-2021

A multilayer network model of the coevolution of the spread of a disease and competing opinions

Kaiyan Peng

Zheng Lu

Vanessa Lin

Michael R. Lindstrom
The University of Texas Rio Grande Valley, mike.lindstrom@utrgv.edu

Christian Parkinson

See next page for additional authors

Recommended Citation

Peng, K., Lu, Z., Lin, V., Lindstrom, M.R., Parkinson, C., Wang, C., Bertozzi, A.L. and Porter, M.A., 2021. A multilayer network model of the coevolution of the spread of a disease and competing opinions. Mathematical Models and Methods in Applied Sciences, 31(12), pp.2455-2494. https://doi.org/10.1142/S0218202521500536

OPEN ACCESS
Mathematical Models and Methods in Applied Sciences
Vol. 31, No. 12 (2021) 2455–2494

DOI: 10.1142/S0218202521500536

A multilayer network model of the coevolution of the spread of a disease and competing opinions

Kaiyan Peng[*,**,‡‡‡], Zheng Lu[†,††], Vanessa Lin[‡,‡‡], Michael R. Lindstrom[*,§§], Christian Parkinson[§,¶¶], Chuntian Wang[¶,‖‖], Andrea L. Bertozzi[*,***] and Mason A. Porter[*,‖,†††]

[*]*Department of Mathematics, University of California, Los Angeles, 520 Portola Plaza, Los Angeles, California 90095, USA*

[†]*Department of Mathematics, University of Wisconsin-Madison, 480 Lincoln Drive, Madison, Wisconsin 53706, USA*

[‡]*Department of Mathematics, University of North Carolina at Chapel Hill, 120 E. Cameron Avenue, Chapel Hill, North Carolina 27599, USA*

[§]*Department of Mathematics, University of Arizona, 617 N. Santa Rita Ave, Tucson, Arizona 85721, USA*

[¶]*Department of Mathematics, The University of Alabama, 505 Hackberry Lane, Tuscaloosa, Alabama 35401, USA*

[‖]*Santa Fe Institute, 1399 Hyde Park Road, Santa Fe, NM 87501, USA*

[**]*kaiyanpeng@ucla.edu*
[††]*zhenglu@math.wisc.edu*
[‡‡]*vllin@live.unc.edu*
[§§]*mikel@math.ucla.edu*
[¶¶]*chparkin@math.arizona.edu*
[‖‖]*cwang27@ua.edu*
[***]*bertozzi@math.ucla.edu*
[†††]*mason@math.ucla.edu*

[‡‡‡]Corresponding author.

Received 6 July 2021
Revised 7 August 2021
Accepted 15 August 2021
Published 11 December 2021
Communicated by N. Bellomo, F. Brezzi and M. A. J. Chaplain

During the COVID-19 pandemic, conflicting opinions on physical distancing swept across social media, affecting both human behavior and the spread of COVID-19. Inspired by such phenomena, we construct a two-layer multiplex network for the coupled spread of a disease and conflicting opinions. We model each process as a contagion. On one layer, we consider the concurrent evolution of two opinions — pro-physical-distancing and anti-physical-distancing — that compete with each other and have mutual immunity to each other. The disease evolves on the other layer, and individuals are less likely (respectively, more likely) to become infected when they adopt the pro-physical-distancing (respectively, anti-physical-distancing) opinion. We develop approximations of mean-field type by generalizing monolayer pair approximations to multilayer networks; these approximations agree well with Monte Carlo simulations for a broad range of parameters and several network structures. Through numerical simulations, we illustrate the influence of opinion dynamics on the spread of the disease from complex interactions both between the two conflicting opinions and between the opinions and the disease. We find that lengthening the duration that individuals hold an opinion may help suppress disease transmission, and we demonstrate that increasing the cross-layer correlations or intra-layer correlations of node degrees may lead to fewer individuals becoming infected with the disease.

Keywords: Multilayer networks; opinion models; competing opinion dynamics; disease dynamics; pair approximations.

AMS Subject Classification 2020: 91D30, 92D30, 37N25

1. Introduction

Since the outbreak of coronavirus disease 2019 (COVID-19), researchers in numerous disciplines have used diverse approaches to analyze the spread of the disease, forecast its subsequent spread under many scenarios, and investigated strategies to mitigate it.[3,6,19] As cases of COVID-19 escalated, collective compliance with non-pharmaceutical intervention (NPI) measures was vital for dealing with the COVID-19 pandemic in the absence of effective treatments and vaccines.[59] As information — some of which was accurate and some of which was not — flooded social media,[26,72] people adopted different opinions about the implementation of NPI measures.[2] These opinions affect human behavior and ultimately also the spread of diseases. Motivated by these observations, we build a multilayer network model to study disease spreading under the influence of the spread of competing information.

It is important to understand the influence of human behavior on the spread of diseases because these two processes are inextricably coupled.[5,67] The acquisition of prevalence-based and/or belief-based information from publicly available sources and/or individuals' social neighborhoods leads to changes of disease states, disease-state transition rates, and social contact patterns.

A common approach to studying the spread of a disease is as a dynamical system on a network of individuals.[12] This type of model emphasizes the importance

of social contact patterns (typically in the form of physical contacts) and the heterogeneity of individuals. When disease and information spread through different venues — such as face-to-face contacts versus online social platforms like Twitter and Facebook — it is useful to use the formalism of multilayer networks,[43] as one can encode different relationships between people in a population in different layers of such a network. There have been many studies of spreading phenomena on multilayer networks and of how such network structures affect spreading processes.[14,68] We discuss some of these in Sec. 2.1.

Past research has examined whether the spread of information can help contain an epidemic (e.g. through decreased transmission rate, fewer contacts, and/or acquired immunity) by leading to a smaller disease prevalence and/or a smaller basic reproduction number (and hence a reduced probability of a large outbreak of the disease).[24,68] However, as has been striking during the COVID-19 pandemic,[75] how people act on information (and misinformation and disinformation) can also have a negative impact on disease propagation; this undermines the potential benefits of information. For example, there have been many anti-physical-distancing rallies in which protesters flout behavioral intervention measures such as wearing masks and practicing physical distancing. Moreover, such large gatherings can directly cause surges in infections.[25]

Motivated by the mixed effects of information and opinion spreading interacting with the spread of a disease, we study a model in which disease transmission is influenced by two opposing opinions: pro-physical-distancing (which we sometimes write simply as "pro" as a shorthand) and anti-physical-distancing (which we sometimes write as "anti"). Following Ref. 32, we consider a two-layer multiplex network (a particular type of multilayer network[43]) with interactions between the spread of opinions and a disease. We model the simultaneous evolution of two competing opinions on one layer of a multiplex network as a contagion process of either susceptible–infectious–recovered (SIR)[40] or susceptible–infectious–recovered–susceptible (SIRS) form, with opinion adoption that occurs between susceptible and infectious individuals. Similar models have been proposed for studying competing diseases[38,49] and ideas.[70] A disease spreads on the other layer (a physical layer) of the multiplex network; the connections in this physical layer encode in-person social contacts. The disease transmission rate depends on the opinions of the individuals.

In our model, we investigate which opinion has greater influence, which we evaluate based on the disease's final epidemic size (i.e. the number of individuals who catch the disease during the disease outbreak). We generate networks using configuration-model networks[21] and their extensions.[48] We demonstrate complex interactions between the two opinions and (because of ensuing behavioral changes, which lead to changes in the network of in-person social contacts) between the opinions and the disease. We explore how the influence of opinions is affected by various factors, including opinion-contagion parameters and network structures.

We derive a mean-field description, in the form of a pair approximation, of our multilayer dynamical system for the expected values of population-scale quantities,

because it is costly to conduct direct simulations of the full stochastic model with a large population. Many approximation methods have been developed for contagion dynamics on monolayer networks (i.e. ordinary graphs),[42] including edge-based compartmental modeling,[50] pair approximations,[39] effective-degree approximations,[46] and approximate master equations.[28,29] In this paper, we use a degree-based pair approximation[17] and generalize it to our multiplex system. In a pair approximation, one examines the various types of pairs in a system and approximates higher-order structures using moment closure.[44] Different pair approximations entail different choices when performing moment closure. Our approximation scheme incorporates dynamical correlations both within and across the layers of a multiplex network. To capture the influence of opinions on individuals' susceptibility to a disease, we also define effective transmission rates that take the form of time-dependent functions of the distribution of opinions in populations of interest. We develop approximations of the effective transmission rates based on the numbers of various types of pairs. Our numerical simulations reveal that our approximate system is able to capture the influence of the spread of opinions on disease spread for population-scale quantities. We find that the time evolution of the expected numbers of individuals in different states in our pair approximation match very well with simulations on a variety of networks with different degree distributions and degree–degree correlations.

Our paper proceeds as follows. In Sec. 2, we discuss prior work and relevant background information and then present our first model. In this model, opinions follow an SIR process. The disease follows an extended SIR process in which people who adopt the pro-physical-distancing opinion (respectively, anti-physical-distancing opinion) have a reduced (respectively, increased) disease transmission rate in comparison to a baseline. In Sec. 3, we assume that the SIR process occurs on a fully-mixed population, yielding a description of our system in terms of a small set of coupled ordinary differential equations (ODEs). In this ODE system, we observe some influence of opinion dynamics on the spread of the disease, but this framework does not include the effects of social contacts. In Sec. 4, we incorporate social contact structures between individuals to yield a dynamical system on a network. We derive a pair approximation for this network model. In Sec. 5, we conduct stochastic simulations of this network model to investigate the influence of the contagion parameters and network structures on the dynamics of the system. In Sec. 6, we generalize our dynamical system by considering an SIRS process for opinion spreading. We conclude in Sec. 7.

2. Background and Modeling

We discuss prior work and background information in Sec. 2.1, and we present our initial model in Sec. 2.2. In this model, we consider a two-layer multiplex network with a disease that spreads on one layer and competing opinions that spread on the other layer. We specify network structures in Sec. 5.

2.1. *Background*

A variety of previous work has examined the influence of social behavior on disease transmission.[24,67] We seek to do this in a way that incorporates the effects of network structures on the spread of disease.[42,60] We consider a social network of individuals (which are represented by nodes) and in-person social contacts (which are represented by edges) between them. The importance of such social contact patterns on dynamical processes has long been recognized,[16] and there has been extensive research on the influence of network structures on the spread of infectious diseases.[56] There is also a large body of work on the spread of social phenomena,[45] including the dissemination of information[9] and the adoption of behaviors,[4] which are often modeled as contagion processes that are similar to disease spread.[8,30] (See Refs. 35 and 71 for discussions of when social contagions resemble and do not resemble contagions of infectious diseases.) In particular, interactions between peers strongly influence the dynamics that unfold on a network.

To give further context for our work, we briefly mention prior investigations on the coevolution of diseases with behavior, awareness, and/or opinions on multilayer networks.[67,68] In particular, many researchers have examined how the spread of awareness can suppress the spread of a disease. Funk *et al.*[23] developed a coevolution model in which individuals acquire different levels of awareness of a disease either by becoming infected or by communicating with their neighbors. In their model, individuals are less susceptible to infection by a disease when they have a higher level of awareness. Subsequently, Funk *et al.*[22] simplified the above model so that individuals are either aware or unaware of a disease, in analogy to the infectious and susceptible states (i.e. "compartments") of a traditional susceptible–infectious–susceptible (SIS) model of disease spread.[11] A similar model was proposed by Granell *et al.*[31,32] Subsequent research has generalized these ideas by modeling the spread of a disease and information using other dyamical systems, such as by modeling disease spread with an SIR model[69] and modeling information transmission with a threshold model[33,34] or a generalized Maki–Thompson rumor model.[13] Other works have examined the influence of global information and mass media,[32,61] the relative speeds of the dynamics of information spread and disease spread,[13,66] and heterogeneous risk perceptions of disease spread.[55,74] Researchers have also incorporated time-varying networks when studying the combined spread of disease and information, such as by coupling an activity-driven information layer with a time-independent disease layer[34] or a time-independent information layer with an adaptive physical layer.[58] Additionally, evolutionary game theory has been used to study decision-making in the presence of government-mandated interventions, socioeconomic costs, perceived infection risks, and social influence.[73]

During the COVID-19 pandemic, content and discussions on social media have played a prominent role. On one hand, social media can help rapidly disseminate transparent and accessible information about policy and scientific findings, and it gives crucial ways to advocate guidance such as mask-wearing and physical distancing.[47] On the other hand, social media also allows the pervasive spread of

misinformation and disinformation, leading to so-called *infodemics*, which refer to epidemics of information.[26,72] Distortion and inaccurate information can impair people's mental and physical health,[62] trigger anxiety and distrust, and ultimately lead to a worse situation for disease spread due to poor compliance with prevention measures. As information floods social media, opposing opinions about physical distancing and other intervention methods develop and propagate rapidly to many people.

Several recent works have examined competing opinion dynamics. Johnson *et al.*[36] studied the evolution of anti-vaccine and pro-vaccine clusters of people on Facebook. She *et al.*[64] examined an opinion model with continuous-valued opinions to study the beliefs of different communities about the severity of disease spread with both cooperative and antagonistic opinion spreading. Epstein *et al.*[18] used compartmental models to study the fear of infection and the fear of vaccines. Johnston and Pell[37] examined the fear of infection and frustration with physical distancing.

2.2. *Our model*

We study the spread of a disease and two competing opinions on a two-layer multiplex network with one physical layer (where the disease spreads) and one information layer (where opinions spread). We assume that all individuals are present in both layers, and we ignore demographic processes such as birth, death, and migration. We model each layer as an undirected, unweighted, simple graph; we couple the two layers to each other by connecting nodes that correspond to the same individual. The edges within a layer are called "intra-layer edges"; they encode in-person contacts in the physical layer and information-exchange channels (especially on social media) in the information layer. An individual can have different neighboring individuals (i.e. adjacent nodes) in the two layers, and their number of neighbors (i.e. their degree) can also be different in the two layers. In Sec. 5, we give further details about the network structure and we explore the influence of inter-layer and intra-layer structure on opinion and disease dynamics. In Secs. 2–5, we use SIR dynamics[40] for each process and associate nodes in the physical layer with individuals' health states and nodes in the information layer with their opinions about physical distancing. In Sec. 6, we extend our model by modeling the spread of opinions as an SIRS process. In all versions of our model, we treat each process as a continuous-time Markov chain. We detail how the disease-spread and opinion-spread processes operate and interact in Secs. 2.2.1 and 2.2.2. In Table 1, we summarize the key parameters of our model.

2.2.1. *Information layer*

Two competing social contagions, which model pro-physical-distancing and anti-physical-distancing opinions, spread concurrently on the information layer. We

Table 1. Key parameters in our model of coupled opinion spread and disease spread. In (a), the first column gives the parameters of the opinion dynamics that are related to pro-physical-distancing and the second column gives the parameters that are related to anti-physical-distancing. We use the subscript "info" when the two opinions share parameters; we indicate these parameters in the third column. In (b), each column indicates the parameters of the disease dynamics when individuals adopt the corresponding opinions.

(a) Parameters for dynamics (of opinion adoption) on the information layer.			
	Pro	Anti	Shared by pro and anti
Transmission rate	β_{pro}	β_{anti}	β_{info}
Recovery rate	γ_{pro}	γ_{anti}	γ_{info}
Immunity-loss rate	τ		

(b) Parameters for dynamics (of disease spread) on the physical layer.			
Opinion / Parameter	U or R_{info}	A	P
Transmission rate	β_{phy}	$\alpha_{\text{anti}}\beta_{\text{phy}}$	$\alpha_{\text{pro}}\beta_{\text{phy}}$
Recovery rate	γ_{phy}		

use P (respectively, A) to denote the pro-physical-distancing (respectively, anti-physical-distancing) state in which individuals both adopt the associated opinion and actively advocate the corresponding behavior. Uninformed (U) individuals are susceptible to both opinions and transition to the P state or A state at rates of β_{pro} and β_{anti}, respectively, by communicating with neighbors in the corresponding states. We suppose that people who adopt either behavior can become weary of acting unusually in comparison with life without a disease epidemic, and they then become less passionate about maintaining their current conduct. We assume that individuals in the P state and A state transition to the recovered (R_{info}) state at rates of γ_{pro} and γ_{anti}, respectively. After this transition occurs, these individuals practice the same behavior as individuals in the uninformed group, but they are resistant to future influence from neighbors. When the two opinions share the same parameters, we use the subscript "info" (see Table 1). We make the assumption of permanent mutual immunity[38]: once an uninformed individual adopts one opinion, it can no longer be influenced by the other opinion. Therefore, upon recovery, it enters the R_{info} state. Because the pro- and anti-physical-distancing opinions are opposing opinions, it is reasonable to assume that individuals do not adopt both behaviors simultaneously. We relax the assumption of permanent immunity in Sec. 6. In Fig. 1, we show the compartment flow diagram of the opinion dynamics.

2.2.2. *Physical layer*

We model the spread of a contagious disease on the physical layer as an SIR-like process. The key difference from a standard SIR contagion is that susceptible nodes have transmission rates that depend on their opinion states.[23,31] We divide susceptible nodes into three types: (1) nodes that do not hold any opinion (i.e. their opinions are in the U state or the R_{info} state) experience the baseline transmission rate β_{phy}; (2) nodes that hold the pro-physical-distancing opinion experience

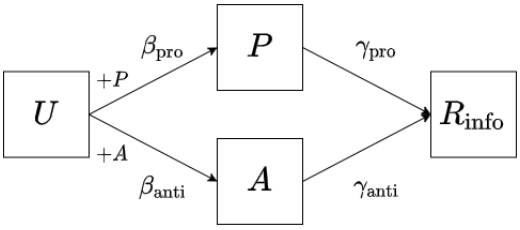

Fig. 1. Schematic illustration of the (opinion-spreading) dynamics on the information layer of a two-layer multiplex network. There are four states in the information layer: uninformed (U), pro-physical-distancing (P), anti-physical-distancing (A), and recovered (R_{info}). Nodes in state U transition to state P (respectively, A) at a rate of β_{pro} (respectively, β_{anti}) by communicating with neighbors in state P (respectively, A). We use "$+P$" (respectively, "$+A$") to emphasize that state transitions occur under the influence of neighbors in P (respectively, A). Nodes in state P (respectively, A) transition to state R_{info} at a rate of γ_{pro} (respectively, γ_{anti}).

a reduced transmission rate $\beta_{\text{phy, pro}} = \alpha_{\text{pro}}\beta_{\text{phy}}$, with $\alpha_{\text{pro}} \leq 1$; and (3) nodes that hold the anti-physical-distancing opinion experience an increased transmission rate $\beta_{\text{phy, anti}} = \alpha_{\text{anti}}\beta_{\text{phy}}$, with $\alpha_{\text{anti}} \geq 1$. We refer to α_{pro} and α_{anti} as "influence coefficients". To model the effects of competing opinions on disease spread, it seems appropriate to study an adaptive network[60] in which structure coevolves with node states. For example, individuals who hold an anti-physical-distancing opinion may have more contacts than other people. However, it is difficult to analyze such a model. Therefore, for simplicity, we assume that individuals who hold the anti-physical-distancing opinion in our model have a higher risk of contracting the disease than the baseline through a higher transmission rate. We make an analogous assumption for nodes that hold the pro-physical-distancing opinion. Infected individuals (which we assume to be the same as infectious individuals) recover at rate γ_{phy}. We show the compartment flow diagram of the disease dynamics in Fig. 2.

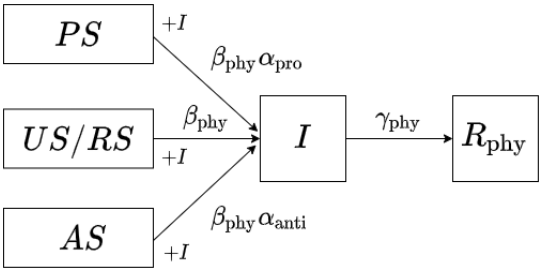

Fig. 2. Schematic illustration of the (disease-spreading) dynamics on the physical layer of a two-layer multiplex network. There are three states in the physical layer: susceptible (S), infectious (I), and recovered (R_{phy}). Based on the opinion states of the node, we further divide the S state into PS, AS, and US/RS. Nodes in state S transition to state I through in-person social contacts with infectious neighbors (which we emphasize with "$+I$") at rates that we mark close to the corresponding arrow. Nodes in state I recover at a rate of γ_{phy}.

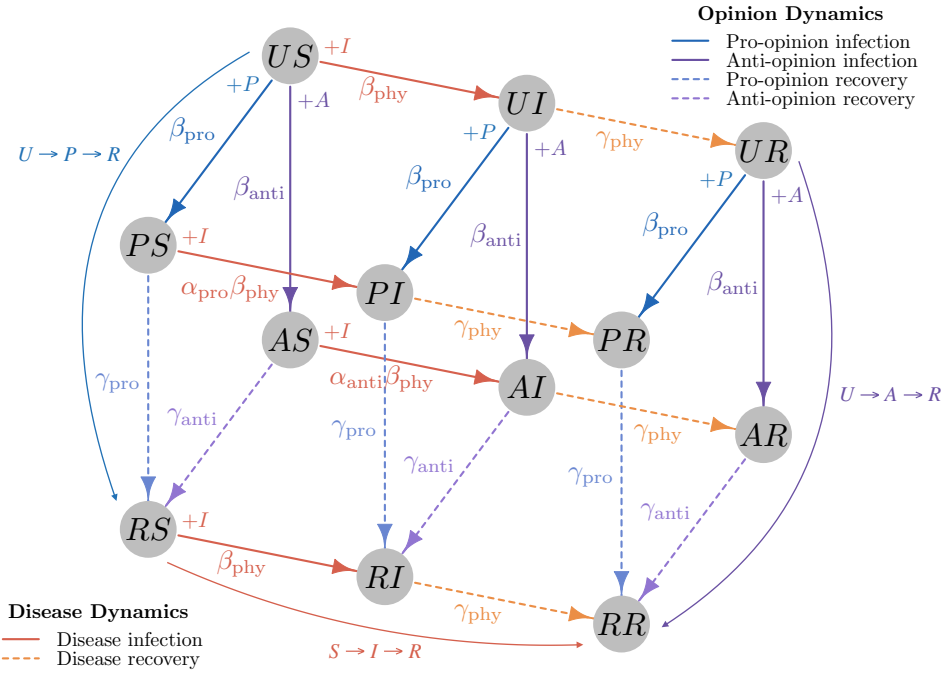

Fig. 3. (Color online) Schematic illustration of our model, with dynamics on both the information layer and the physical layer. The disks indicate the possible states (i.e. compartments) of a node. In each state, the first letter (U, P, A, or R) indicates the opinion state and the second letter (S, I, or R) indicates the disease state. The arrows indicate the possible state transitions.

Combining the dynamics on the two layers, we use two letters to describe the full profile of an individual; the first one indicates a node's opinion state, and the second one indicates its disease state. To simplify our notation, we also drop the subscript for the R compartment, as the order of the two letters in a state already indicates whether we are referring to the opinion state or the disease state. There are a total of 12 possible states (i.e. compartments). We show the complete compartment flow diagram for our model in Fig. 3. For convenience, we use the same notation for the state of a node and the set of nodes in a specified state throughout this paper.

3. Dynamics on a Fully-Mixed Population

We first study our model in a fully-mixed population, which yields a small set of coupled ODEs.[11] We ignore contact patterns in both the information layer and the physical layer. Additionally, in every small time interval, we assume that each node interacts with other nodes in the same layer uniformly at random. We refer to this assumption as the "random-mixing assumption". In each time interval, we also assign each node in one layer to a counterpart node in the other layer uniformly at random (without replacement). We refer to this assumption as the

"random-recoupling assumption". Throughout this paper, we use $[X] = \mathbb{E}[X]/N$ as the shorthand notation for the expectation of the random variable X divided by the population size N. Using the law of mass action, we obtain the following population-level dynamics:

$$\begin{aligned}
\frac{d}{dt}[|U|] &= -\frac{\beta_{\text{pro}}}{N}[|U| \times |P|] - \frac{\beta_{\text{anti}}}{N}[|U| \times |A|]\,,\\
\frac{d}{dt}[|P|] &= \frac{\beta_{\text{pro}}}{N}[|U| \times |P|] - \gamma_{\text{pro}}[|P|]\,,\\
\frac{d}{dt}[|A|] &= \frac{\beta_{\text{anti}}}{N}[|U| \times |A|] - \gamma_{\text{anti}}[|A|]\,,\\
\frac{d}{dt}[|R_{\text{info}}|] &= \gamma_{\text{pro}}[|P|] + \gamma_{\text{anti}}[|A|]\,,\\
\frac{d}{dt}[|S|] &= -\frac{\beta^*}{N}[|S| \times |I|]\,,\\
\frac{d}{dt}[|I|] &= \frac{\beta^*}{N}[|S| \times |I|] - \gamma_{\text{phy}}[|I|]\,,\\
\frac{d}{dt}[|R_{\text{phy}}|] &= \gamma_{\text{phy}}[|I|]\,,
\end{aligned} \tag{3.1}$$

where we use $|\cdot|$ to denote cardinality and

$$\beta^* = ([|P|]\alpha_{\text{pro}} + [|A|]\alpha_{\text{anti}} + 1 - [|A|] - [|P|])\beta_{\text{phy}}\,.$$

The first four equations describe the opinion dynamics. Uninformed nodes may adopt the pro- or anti-physical-distancing opinions by interacting with a node in the corresponding state. If a node adopts an opinion, it then can spread that opinion to its neighbors. The last four equations in (3.1) describe disease dynamics as a variant of the standard SIR model. The quantity β^* is the effective transmission rate; it depends on the relative prevalence of nodes in states P and A. To close the system, we approximate the expectations of products with the products of expectations. For example,

$$\frac{1}{N}[|U| \times |P|] \approx [|U|] \times [|P|]\,.$$

This provides a good approximation when N is large. Henceforth, we omit $|\cdot|$ to simplify our notation.

Consider the special case in which the transmission rate β_{pro}, recovery rate γ_{pro}, and initial population proportion of the pro-physical-distancing opinion are the same as the corresponding parameters for the anti-physical-distancing opinion. In this case, the effective transmission rate is $\beta^* = ([P](\alpha_{\text{anti}} + \alpha_{\text{pro}} - 2) + 1)\beta_{\text{phy}}$. Because $[P] \geq 0$, it follows that $\beta^* \geq \beta_{\text{phy}}$ if and only if $\alpha_{\text{anti}} + \alpha_{\text{pro}} \geq 2$. Therefore, the spread of opinions always leads to more infections of the disease. If $\alpha_{\text{anti}} + \alpha_{\text{pro}} = 2$, the opinion dynamics has no effect on disease spread. This conclusion relies on the random-recoupling assumption, which implies that the

information-layer counterpart of any physical-layer node is equally likely to be in any given opinion state. Because individuals hold an opinion for some time, the sign of $\alpha_{\text{anti}} + \alpha_{\text{pro}} - 2$ alone does not determine whether the influence of opinions leads to more infections or fewer infections when we consider the effects of network structure in Sec. 5.

The epidemic threshold in a standard SIR model of disease spread is characterized by the basic reproduction number[11,15] $R_0 = \beta/\gamma$, which is the mean number of secondary infections that arise from a single infectious individual in a population in which everyone else is susceptible. An epidemic outbreak of the disease occurs if $R_0 > 1$. In our model, suppose that we start with a population in which most people are susceptible and uninformed about the disease. In this case, β^* is close to β. In the limit in which the population becomes infinite with a vanishing fraction of people initially holding any opinion, the epidemic threshold is the same as in the standard SIR model and it is independent of the information layer. However, this conclusion does not hold if too many people hold some opinion about the disease at time 0.

Although an information contagion may not affect the epidemic threshold for the spread of a disease, it can still have a large impact on the disease's prevalence if an epidemic outbreak occurs. In Fig. 4, we show an illustrative example to demonstrate how the information layer can affect the spread of a disease. For simplicity, we suppose that the pro- and anti-physical-distancing opinions share the same contagion parameters. Figure 4(a) shows an example in which we fix the parameters in the physical layer (on which the disease spreads) and investigate the effect of the opinion recovery rate on the final epidemic size (i.e. the total number of people who become infectious during the outbreak). Because we fix $\beta_{\text{info}} = 2$, the opinion contagion grows into an outbreak if γ_{info} is less than approximately 2. Consequently, all curves for the final epidemic size converge to the same value when γ_{info} is at least approximately 2. To assist our exposition, we use the term "basic size" to indicate the final epidemic size when the disease spreads independently of opinions. Because the effective transmission rate β^* satisfies $\beta^* \geq \beta_{\text{phy}}$, we expect the final epidemic size to be no smaller than the basic size.

The final epidemic size is affected by the prevalence of the nodes in states P and A and the relative spreading speeds of the opinions and the disease. As we increase γ_{info} in Fig. 4(a), the final epidemic size tends to decrease, but it grows at first before decreasing to the basic size. To understand this, we compare the spreading dynamics on the two layers (see Figs. 4(b) and 4(c)). Increasing γ_{info} leads to a reduction in the number of people in compartments P and A, which reduces the adverse influence from the information layer and results in fewer people becoming infected. Increasing γ_{info} also postpones the time that it takes for the physical layer to achieve herd immunity. Specifically, it takes longer for the I compartment to reach its maximum size. We also see that increasing γ_{info} from 1 to 1.5 shortens the time difference between the opinion-prevalence peak and the disease-prevalence peak. As the two peaks become closer to each other, we observe transient growth in

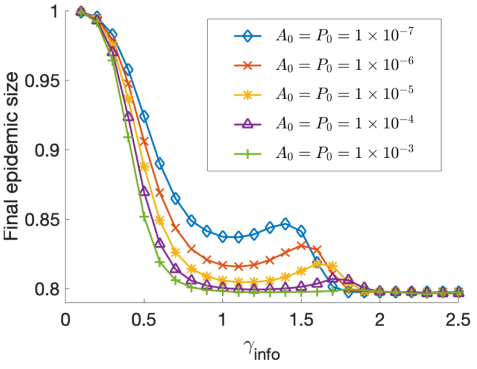

(a) Final epidemic size

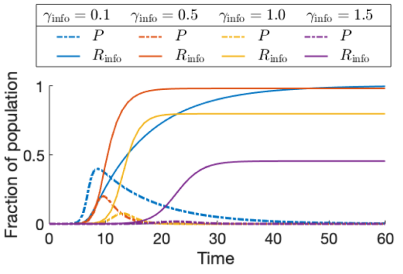

(b) Information layer

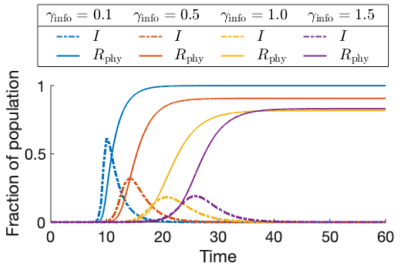

(c) Physical layer

Fig. 4. (Color online) The influence of the information layer on the physical layer depends on the opinion recovery rates. (a) Effects of γ_{info} on the final epidemic size for different initial conditions. For simplicity, we suppose that the pro- and anti-physical-distancing opinions share the same contagion parameters for all examples in the paper. That is, $\beta_{\text{anti}} = \beta_{\text{pro}}$ (which we denote by β_{info}), $\gamma_{\text{anti}} = \gamma_{\text{pro}}$ (which we denote by γ_{info}), and $A_0 = P_0$, where $A_0 = [A](0)$ and $P_0 = [P](0)$. In the physical layer, we uniformly randomly infect a fraction $I_0 = [I](0) = 1 \times 10^{-6}$ of the population; the rest of the population starts in the susceptible state. The other parameters are $\beta_{\text{phy}} = 1$, $\gamma_{\text{phy}} = 0.5$, $\alpha_{\text{pro}} = 0.1$, $\alpha_{\text{anti}} = 10$, and $\beta_{\text{info}} = 2$. To help explain the non-monotonic curve in panel (a), we fix $P_0 = A_0 = 1 \times 10^{-6}$ and examine different values of γ_{info}. We show the ensuing dynamics of the fraction of the population in the P and R_{info} compartments in panel (b) and the fraction of the population in the I and R_{phy} compartments in panel (c).

Fig. 4(a). When we change the initial numbers of individuals in states A and P while fixing the initial numbers of individuals in state I in Fig. 4(a), we effectively change the relative starting times of the opinion dynamics versus the disease dynamics, leading to differences between the curves.

4. Dynamics on a Population with Network Structure

The random-mixing assumption and random-recoupling assumption in Sec. 3 ignore contact patterns and oversimplify the dynamics of the spread of opinions and diseases. In real life, both in-person contacts and online interactions have intricate structural patterns[53] that are far from homogeneous. Moreover, the random-recoupling assumption mixes the effects of the pro- and anti-physical-distancing opinions in a naive way and leads to features that contradict what we observe in individual-level simulations. Consequently, it is necessary to differentiate between

different opinion states within the susceptible population and analyze the dynamics of the 12 compartments in Fig. 3. Starting in this section, we incorporate network structure into our model and study the resulting dynamics in detail.

We develop a mean-field description of our dynamical system by generalizing the degree-based pair approximation of Eames and Keeling[17] to coupled dynamics on multilayer networks. We assume that all nodes with the same degree are statistically equivalent, and we estimate the expected number of nodes and the expected number of dyads (i.e. pairs of nodes that are attached to the same edge) for each degree and each compartment[42] using a closure model. We examine the dynamics of the spread of opinions and a disease using a mean of an ensemble of networks.[56,60] We first develop an exact ODE system that involves single, pair, and triple terms based on the law of mass action. This system also depends on a set of time-dependent effective transmission rates. We close the system by approximating triple terms and the effective transmission rates using pair terms. The number of equations in the system depends on the number of distinct degrees and is independent of the population size.

4.1. *Our dynamical system at the level of triples*

Recall that we use two adjacent letters YX to describe the state (i.e. compartment) of an individual, where the first letter indicates the information layer and the second letter indicates the disease layer. The two intra-layer degrees of a node are its numbers of neighbors in the two layers. We are interested only in intra-layer degrees, so we treat our multiplex networks as edge-colored multigraphs.[43] We use $Y_{k_1}X_{k_2}$ to refer to nodes in state YX with degree k_1 in the information layer and degree k_2 in the physical layer. We write the expected density of these nodes as $[Y_{k_1}X_{k_2}]$. To simplify our notation, we drop subscripts to indicate summation over all possible degrees. For example, $[YX_{k_2}] = \sum_{k_1}[Y_{k_1}X_{k_2}]$. For ease of notation, we use one letter and thereby specify the state only in that layer when the context is clear. For example, S_{k_2} refers to susceptible nodes with degree k_2 in the physical layer and $[S_{k_2}]$ refers to the expected density of these nodes.

To track the states of the neighbors of a node, we write the expected normalized count of the dyads of nodes with states $\mathcal{S}_1$ and $\mathcal{S}_2$ as $[\mathcal{S}_1 \circ \mathcal{S}_2]$, where $\circ$ denotes an edge and the normalized count is the number of dyads divided by the population size. The layer of a dyad is clear from the context. For example, $[U_{k_1}S_{k_2} \circ I]$ represents the expected normalized count of dyads in the physical layer for which one end is attached to a $U_{k_1}S_{k_2}$ node and the other end is attached to an infectious node.

Given the above notation and definitions, the time evolution of the expected density of each compartment is

$$\frac{d}{dt}[U_{k_1}S_{k_2}] = -[U_{k_1}S_{k_2} \circ I]\beta_{\text{phy}} - [U_{k_1}S_{k_2} \circ A]\beta_{\text{anti}} - [U_{k_1}S_{k_2} \circ P]\beta_{\text{pro}}\,,$$

$$
\begin{aligned}
\frac{d}{dt}[U_{k_1}I_{k_2}] &= [U_{k_1}S_{k_2}\circ I]\beta_{\text{phy}} - [U_{k_1}I_{k_2}]\gamma_{\text{phy}} - [U_{k_1}I_{k_2}\circ A]\beta_{\text{anti}} \\
&\quad - [U_{k_1}I_{k_2}\circ P]\beta_{\text{pro}}\,, \\
\frac{d}{dt}[U_{k_1}R_{k_2}] &= [U_{k_1}I_{k_2}]\gamma_{\text{phy}} - [U_{k_1}R_{k_2}\circ A]\beta_{\text{anti}} - [U_{k_1}R_{k_2}\circ P]\beta_{\text{pro}}\,, \\
\frac{d}{dt}[A_{k_1}S_{k_2}] &= -[A_{k_1}S_{k_2}\circ I]\beta_{\text{phy}}\alpha_{\text{anti}} + [U_{k_1}S_{k_2}\circ A]\beta_{\text{anti}} - [A_{k_1}S_{k_2}]\gamma_{\text{anti}}\,, \\
\frac{d}{dt}[A_{k_1}I_{k_2}] &= [A_{k_1}S_{k_2}\circ I]\beta_{\text{phy}}\alpha_{\text{anti}} - [A_{k_1}I_{k_2}](\gamma_{\text{phy}}+\gamma_{\text{anti}}) + [U_{k_1}I_{k_2}\circ A]\beta_{\text{anti}}\,, \\
\frac{d}{dt}[A_{k_1}R_{k_2}] &= [A_{k_1}I_{k_2}]\gamma_{\text{phy}} + [U_{k_1}R_{k_2}\circ A]\beta_{\text{anti}} - [A_{k_1}R_{k_2}]\gamma_{\text{anti}}\,, \\
\frac{d}{dt}[P_{k_1}S_{k_2}] &= -[P_{k_1}S_{k_2}\circ I]\beta_{\text{phy}}\alpha_{\text{pro}} + [U_{k_1}S_{k_2}\circ P]\beta_{\text{pro}} - [P_{k_1}S_{k_2}]\gamma_{\text{pro}}\,, \\
\frac{d}{dt}[P_{k_1}I_{k_2}] &= [P_{k_1}S_{k_2}\circ I]\beta_{\text{phy}}\alpha_{\text{pro}} - [P_{k_1}I_{k_2}](\gamma_{\text{phy}}+\gamma_{\text{pro}}) + [U_{k_1}I_{k_2}\circ P]\beta_{\text{pro}}\,, \\
\frac{d}{dt}[P_{k_1}R_{k_2}] &= [P_{k_1}I_{k_2}]\gamma_{\text{phy}} + [U_{k_1}R_{k_2}\circ P]\beta_{\text{pro}} - [P_{k_1}R_{k_2}]\gamma_{\text{pro}}\,, \\
\frac{d}{dt}[R_{k_1}S_{k_2}] &= -[R_{k_1}S_{k_2}\circ I]\beta_{\text{phy}} + [A_{k_1}S_{k_2}]\gamma_{\text{anti}} + [P_{k_1}S_{k_2}]\gamma_{\text{pro}}\,, \\
\frac{d}{dt}[R_{k_1}I_{k_2}] &= [R_{k_1}S_{k_2}\circ I]\beta_{\text{phy}} - [R_{k_1}I_{k_2}]\gamma_{\text{phy}} + [A_{k_1}I_{k_2}]\gamma_{\text{anti}} + [P_{k_1}I_{k_2}]\gamma_{\text{pro}}\,.
\end{aligned}
\tag{4.1}
$$

To illustrate the equations in (4.1), we briefly discuss one of them. In the first equation, the expected number of $U_{k_1}S_{k_2}$ nodes decreases as the nodes become infectious or adopt one of the two opinions. The infection rate is proportional to the number of infectious neighbors (or, equivalently, to the number of $U_{k_1}S_{k_2}\circ I_l$ dyads). We do not track the opinion states of those infectious neighbors because we assume that those opinions do not affect the transmission rate of the $U_{k_1}S_{k_2}$ nodes. The same reasoning applies to the other dyads.

We expand the right-hand side of the system (4.1) by tracking the dynamics of node pairs, which depend on the neighbors of both nodes and thus involve triples. Let $[X\circ Y\circ Z]$ denote the expected normalized count of triples in which the center node Y is adjacent to X and to Z. Analogously to the normalized count of a dyad, we define the normalized count of a triple to be the number of triples divided by the population size. The two edges may belong to the same layer or to different layers; this is clear from the context. For example, $U_{k_1}S_{k_2}\circ S_l\circ I$ refers to triples in which the center node S_l has physical-layer neighbors with states $U_{k_1}S_{k_2}$ and I. Additionally, $P\circ U_{k_1}S_{k_2}\circ I_l$ refers to triples in which one edge connects $U_{k_1}S_{k_2}$ and P nodes in the information layer and the other edge connects $U_{k_1}S_{k_2}$ and I_l nodes in the physical layer. We now write the evolution of the expected normalized count

of the dyads in terms of triples terms:

$$
\begin{aligned}
&\frac{d}{dt}[U_{k_1} S_{k_2} \circ I_l] \\
&\quad = [U_{k_1} S_{k_2} \circ S_l \circ I]\hat{\beta}_{l,\,k_2} - ([U_{k_1} S_{k_2} \circ I_l] + [I \circ U_{k_1} S_{k_2} \circ I_l])\beta_{\text{phy}} \\
&\qquad - [U_{k_1} S_{k_2} \circ I_l]\gamma_{\text{phy}} - [P \circ U_{k_1} S_{k_2} \circ I_l]\beta_{\text{pro}} - [A \circ U_{k_1} S_{k_2} \circ I_l]\beta_{\text{anti}}\,, \\
&\frac{d}{dt}[U_{k_1} S_{k_2} \circ S_l] \\
&\quad = -[U_{k_1} S_{k_2} \circ S_l \circ I]\hat{\beta}_{l,\,k_2} - [I \circ U_{k_1} S_{k_2} \circ S_l]\beta_{\text{phy}} \\
&\qquad - [P \circ U_{k_1} S_{k_2} \circ S_l]\beta_{\text{pro}} - [A \circ U_{k_1} S_{k_2} \circ S_l]\beta_{\text{anti}}\,, \\
&\frac{d}{dt}[U_{k_1} S_{k_2} \circ A_l] \\
&\quad = -[P \circ U_{k_1} S_{k_2} \circ A_l]\beta_{\text{pro}} - [U_{k_1} S_{k_2} \circ A_l]\gamma_{\text{anti}} - [I \circ U_{k_1} S_{k_2} \circ A_l]\beta_{\text{phy}} \\
&\qquad + ([U_{k_1} S_{k_2} \circ U_l \circ A] - [U_{k_1} S_{k_2} \circ A_l] - [A \circ U_{k_1} S_{k_2} \circ A_l])\beta_{\text{anti}}\,, \\
&\frac{d}{dt}[U_{k_1} S_{k_2} \circ P_l] \\
&\quad = -[A \circ U_{k_1} S_{k_2} \circ P_l]\beta_{\text{anti}} - [U_{k_1} S_{k_2} \circ P_l]\gamma_{\text{pro}} - [I \circ U_{k_1} S_{k_2} \circ P_l]\beta_{\text{phy}} \\
&\qquad + ([U_{k_1} S_{k_2} \circ U_l \circ P] - [U_{k_1} S_{k_2} \circ P_l] - [P \circ U_{k_1} S_{k_2} \circ P_l])\beta_{\text{pro}}\,, \\
&\frac{d}{dt}[U_{k_1} S_{k_2} \circ U_l] \\
&\quad = -([P \circ U_{k_1} S_{k_2} \circ U_l] + [U_{k_1} S_{k_2} \circ U_l \circ P])\beta_{\text{pro}} - [I \circ U_{k_1} S_{k_2} \circ U_l]\beta_{\text{phy}} \\
&\qquad - ([A \circ U_{k_1} S_{k_2} \circ U_l] + [U_{k_1} S_{k_2} \circ U_l \circ A])\beta_{\text{anti}}\,, \\
&\frac{d}{dt}[U_{k_1} I_{k_2} \circ A_l] \\
&\quad = ([U_{k_1} I_{k_2} \circ U_l \circ A] - [A \circ U_{k_1} I_{k_2} \circ A_l])\beta_{\text{anti}} - [P \circ U_{k_1} I_{k_2} \circ A_l]\beta_{\text{pro}} \\
&\qquad + [I \circ U_{k_1} S_{k_2} \circ A_l]\beta_{\text{phy}} - [U_{k_1} I_{k_2} \circ A_l](\gamma_{\text{phy}} + \gamma_{\text{anti}} + \beta_{\text{anti}})\,, \\
&\frac{d}{dt}[U_{k_1} I_{k_2} \circ P_l] \\
&\quad = ([U_{k_1} I_{k_2} \circ U_l \circ P] - [P \circ U_{k_1} I_{k_2} \circ P_l])\beta_{\text{pro}} - [A \circ U_{k_1} I_{k_2} \circ P_l]\beta_{\text{anti}} \\
&\qquad + [I \circ U_{k_1} S_{k_2} \circ P_l]\beta_{\text{phy}} - [U_{k_1} I_{k_2} \circ P_l](\beta_{\text{pro}} + \gamma_{\text{phy}} + \gamma_{\text{pro}})\,, \\
&\frac{d}{dt}[U_{k_1} I_{k_2} \circ U_l] \\
&\quad = [I \circ U_{k_1} S_{k_2} \circ U_l]\beta_{\text{phy}} - ([A \circ U_{k_1} I_{k_2} \circ U_l] + [U_{k_1} I_{k_2} \circ U_l \circ A])\beta_{\text{anti}} \\
&\qquad - ([U_{k_1} I_{k_2} \circ U_l \circ P] + [P \circ U_{k_1} I_{k_2} \circ U_l])\beta_{\text{pro}} - [U_{k_1} I_{k_2} \circ U_l]\gamma_{\text{phy}}\,,
\end{aligned}
$$

$$
\begin{aligned}
&\frac{d}{dt}[U_{k_1}R_{k_2}\circ A_l]\\
&\quad=[U_{k_1}I_{k_2}\circ A_l]\gamma_{\text{phy}}-[U_{k_1}R_{k_2}\circ A_l]\gamma_{\text{anti}}-[P\circ U_{k_1}R_{k_2}\circ A_l]\beta_{\text{pro}}\\
&\qquad+([U_{k_1}R_{k_2}\circ U_l\circ A]-[U_{k_1}R_{k_2}\circ A_l]-[A\circ U_{k_1}R_{k_2}\circ A_l])\beta_{\text{anti}}\,,\\
&\frac{d}{dt}[U_{k_1}R_{k_2}\circ P_l]\\
&\quad=[U_{k_1}I_{k_2}\circ P_l]\gamma_{\text{phy}}-[U_{k_1}R_{k_2}\circ P_l]\gamma_{\text{pro}}-[A\circ U_{k_1}R_{k_2}\circ P_l]\beta_{\text{anti}}\\
&\qquad+([U_{k_1}R_{k_2}\circ U_l\circ P]-[U_{k_1}R_{k_2}\circ P_l]-[P\circ U_{k_1}R_{k_2}\circ P_l])\beta_{\text{pro}}\,,\\
&\frac{d}{dt}[U_{k_1}R_{k_2}\circ U_l]\\
&\quad=[U_{k_1}I_{k_2}\circ U_l]\gamma_{\text{phy}}-([U_{k_1}R_{k_2}\circ U_l\circ A]+[A\circ U_{k_1}R_{k_2}\circ U_l])\beta_{\text{anti}}\\
&\qquad-([U_{k_1}R_{k_2}\circ U_l\circ P]+[P\circ U_{k_1}R_{k_2}\circ U_l])\beta_{\text{pro}}\,,\\
&\frac{d}{dt}[A_{k_1}S_{k_2}\circ I_l]\\
&\quad=[A\circ U_{k_1}S_{k_2}\circ I_l]\beta_{\text{anti}}-[A_{k_1}S_{k_2}\circ I_l](\gamma_{\text{phy}}+\gamma_{\text{anti}}+\beta_{\text{phy}}\alpha_{\text{anti}})\\
&\qquad+[A_{k_1}S_{k_2}\circ S_l\circ I]\hat{\beta}_{l,\,k_2}-[I\circ A_{k_1}S_{k_2}\circ I_l]\beta_{\text{phy}}\alpha_{\text{anti}}\,,\\
&\frac{d}{dt}[A_{k_1}S_{k_2}\circ S_l]\\
&\quad=-[A_{k_1}S_{k_2}\circ S_l\circ I]\hat{\beta}_{l,\,k_2}-[I\circ A_{k_1}S_{k_2}\circ S_l]\beta_{\text{phy}}\alpha_{\text{anti}}\\
&\qquad+[A\circ U_{k_1}S_{k_2}\circ S_l]\beta_{\text{anti}}-[A_{k_1}S_{k_2}\circ S_l]\gamma_{\text{anti}}\,,\\
&\frac{d}{dt}[P_{k_1}S_{k_2}\circ I_l]\\
&\quad=[P\circ U_{k_1}S_{k_2}\circ I_l]\beta_{\text{pro}}-[P_{k_1}S_{k_2}\circ I_l](\gamma_{\text{phy}}+\gamma_{\text{anti}}+\beta_{\text{phy}}\alpha_{\text{pro}})\\
&\qquad+[P_{k_1}S_{k_2}\circ S_l\circ I]\hat{\beta}_{l,\,k_2}-[I\circ P_{k_1}S_{k_2}\circ I_l]\beta_{\text{phy}}\alpha_{\text{pro}}\,,\\
&\frac{d}{dt}[P_{k_1}S_{k_2}\circ S_l]\\
&\quad=-[P_{k_1}S_{k_2}\circ S_l\circ I]\hat{\beta}_{l,\,k_2}-[I\circ P_{k_1}S_{k_2}\circ S_l]\beta_{\text{phy}}\alpha_{\text{pro}}\\
&\qquad+[P\circ U_{k_1}S_{k_2}\circ S_l]\beta_{\text{pro}}-[P_{k_1}S_{k_2}\circ S_l]\gamma_{\text{pro}}\,,\\
&\frac{d}{dt}[R_{k_1}S_{k_2}\circ I_l]\\
&\quad=[R_{k_1}S_{k_2}\circ S_l\circ I]\hat{\beta}_{l,\,k_2}-([R_{k_1}S_{k_2}\circ I_l]+[I\circ R_{k_1}S_{k_2}\circ I_l])\beta_{\text{phy}}\\
&\qquad-[R_{k_1}S_{k_2}\circ I_l]\gamma_{\text{phy}}+[A_{k_1}S_{k_2}\circ I_l]\gamma_{\text{anti}}+[P_{k_1}S_{k_2}\circ I_l]\gamma_{\text{pro}}\,,\\
&\frac{d}{dt}[R_{k_1}S_{k_2}\circ S_l]\\
&\quad=-[R_{k_1}S_{k_2}\circ S_l\circ I]\hat{\beta}_{l,\,k_2}-[I\circ R_{k_1}S_{k_2}\circ S_l]\beta_{\text{phy}}\\
&\qquad+[A_{k_1}S_{k_2}\circ S_l]\gamma_{\text{anti}}+[P_{k_1}S_{k_2}\circ S_l]\gamma_{\text{pro}}\,,
\end{aligned}
\tag{4.2}
$$

where $\hat{\beta}_{l,k_2}$ is the expected transmission rate of the center node S_l in a triple of the form $YS_{k_2} \circ S_l \circ I$.

One derives the system (4.2) using the same reasoning as in (4.1). For example, consider the first equation in (4.2). The normalized count of the dyads $U_{k_1}S_{k_2} \circ I_l$ decreases as $U_{k_1}S_{k_2}$ nodes adopt one of the two opinions at rate $[P \circ U_{k_1}S_{k_2} \circ I_l]\beta_{\text{pro}} + [A \circ U_{k_1}S_{k_2} \circ I_l]\beta_{\text{anti}}$, is infected by I_l at rate $[U_{k_1}S_{k_2} \circ I_l]\beta_{\text{phy}}$, or is infected by infectious neighbors other than I_l at rate $[I \circ U_{k_1}S_{k_2} \circ I_l]\beta_{\text{phy}}$. The normalized count of $U_{k_1}S_{k_2} \circ I_l$ increases as susceptible neighbors of $U_{k_1}S_{k_2}$ are infected by their infectious neighbors at rate $[U_{k_1}S_{k_2} \circ S_l \circ I]\hat{\beta}_{l,k_2}$. Each dyad in (4.2) has one node whose state we track in only one of the layers. For example, for the dyad $U_{k_1}S_{k_2} \circ S_l$, we do not know the opinion state of node S_l. We need an approximation for the disease transmission rate $\hat{\beta}_{l,k_2}$ when node S_l is infected by a neighbor in state I. In principle, one can track the states of both nodes on both layers and avoid the need for this approximation. However, doing this leads to a higher-dimensional system. We discuss the approximation of $\hat{\beta}_{l,k_2}$ in Sec. 4.3.

In principle, one can also work out the right-hand sides for the evolution of the expected normalized counts of the triple terms. These incorporate quadruple terms, and if we expand those terms and keep expanding expressions for the evolution of progressively larger network motifs (i.e. connected subgraphs), we eventually obtain an exact dynamical system. However, it is very high-dimensional and difficult to study. Therefore, we approximate the triple terms with pair terms on the right-hand sides of (4.2) using the approach in Ref. 17.

4.2. *Closure of the triple terms*

For a given type of triple $X \circ Y_k \circ Z$, we assume that the neighbors of all Y_k nodes are interchangeable. Therefore, every neighbor has the same probability of being in a given state (e.g. state X).

If both edges are in the same layer, then for nodes X and Z that are adjacent to a center degree-k node in state Y in the same layer, it follows that

$$[X \circ Y_k \circ Z] \approx k(k-1)[Y_k]\frac{[X \circ Y_k]}{k[Y_k]}\frac{[Y_k \circ Z]}{k[Y_k]} = \frac{k-1}{k}\frac{[X \circ Y_k][Y_k \circ Z]}{[Y_k]}. \tag{4.3}$$

Intuitively, nodes in state Y_k have $k[Y_k]$ edges; an expected fraction $\frac{[X \circ Y_k]}{k[Y_k]}$ of these edges are attached to nodes in state X, and an expected fraction $\frac{[Y_k \circ Z]}{k[Y_k]}$ of these edges are attached to nodes in state Z. Therefore, if we choose a node in state Y_k uniformly at random, the probability that two uniformly random neighbors of that node are in states X and Z is approximately $\frac{[X \circ Y_k]}{k[Y_k]} \times \frac{[Y_k \circ Z]}{k[Y_k]}$ when N is large. Because there are $k(k-1)$ ways to choose the two neighbors, we obtain (4.3). As

concrete examples,

$$[U_{k_1}S_{k_2}\circ S_l\circ I]\approx\frac{l-1}{l}\frac{[U_{k_1}S_{k_2}\circ S_l][S_l\circ I]}{[S_l]}\,,$$

$$[I\circ U_{k_1}S_{k_2}\circ S_l]\approx\frac{k_2-1}{k_2}\frac{[I\circ U_{k_1}S_{k_2}][U_{k_1}S_{k_2}\circ S_l]}{[U_{k_1}S_{k_2}]}\,,$$

$$[A\circ U_{k_1}S_{k_2}\circ A_l]\approx\frac{k_1-1}{k_1}\frac{[A\circ U_{k_1}S_{k_2}][U_{k_1}S_{k_2}\circ A_l]}{[U_{k_1}S_{k_2}]}\,.$$

Suppose instead that the two edges that connect the center node $Y_{1,k_1}Y_{2,k_2}$ to nodes in states X and Z are in different layers. If the node in state X is in the information layer and the node in state Z is in the physical layer, we obtain

$$\begin{aligned}[X\circ Y_{1,k_1}Y_{2,k_2}\circ Z]&\approx k_1k_2[Y_{1,k_1}Y_{2,k_2}]\frac{[X\circ Y_{1,k_1}Y_{2,k_2}]}{k_1[Y_{1,k_1}Y_{2,k_2}]}\frac{[Y_{1,k_1}Y_{2,k_2}\circ Z]}{k_2[Y_{1,k_1}Y_{2,k_2}]}\\&=\frac{[X\circ Y_{1,k_1}Y_{2,k_2}][Y_{1,k_1}Y_{2,k_2}\circ Z]}{[Y_{1,k_1}Y_{2,k_2}]}\,.\end{aligned}$$

For example,

$$[P\circ U_{k_1}S_{k_2}\circ I_l]\approx\frac{[P\circ U_{k_1}S_{k_2}][U_{k_1}S_{k_2}\circ I_l]}{[U_{k_1}S_{k_2}]}\,.$$

One can work out approximations for the other triple terms similarly.

4.3. *Approximate transmission rate*

To close equations (4.1)–(4.2), we need to find an approximation of $\hat{\beta}_{l,\,k_2}$, which is the expected transmission rate of the center node in triples of the form $YS_{k_2}\circ S_l\circ I$. We need to approximate the opinion distribution in each population of interest. The random-recoupling assumption in Sec. 3 corresponds to setting

$$\hat{\beta}_{l,\,k_2}\approx([U]+[A]\alpha_{\rm anti}+[P]\alpha_{\rm pro}+[R])\beta_{\rm phy}\,. \tag{4.4}$$

However, it is possible to keep track of corresponding nodes in the two layers. A naive approach is to weight the influence coefficients based on the densities of nodes with different opinion states among the S_l nodes. That is,

$$\hat{\beta}_{l,\,k_2}\approx\frac{[US_l]+[AS_l]\alpha_{\rm anti}+[PS_l]\alpha_{\rm pro}+[RS_l]}{[S_l]}\beta_{\rm phy}\,. \tag{4.5}$$

However, the approximation (4.5) ignores the fact that the S_l node of interest has both an intra-layer neighbor in state S and an intra-layer neighbor in state I. Incorporating this neighborhood information yields the approximation

$$\begin{aligned}\hat{\beta}_{l,\,k_2}\approx\big([S_{k_2}\circ US_l\circ I]+[S_{k_2}\circ AS_l\circ I]\alpha_{\rm anti}\\+[S_{k_2}\circ PS_l\circ I]\alpha_{\rm pro}+[S_{k_2}\circ RS_l\circ I]\big)\times\frac{\beta_{\rm phy}}{[S_{k_2}\circ S_l\circ I]}\,.\end{aligned} \tag{4.6}$$

We approximate the triples in (4.6) with our pair approximation:

$$[S_{k_2} \circ U_k S_l \circ I] \approx \frac{l-1}{l} \frac{[U_k S_l \circ S_{k_2}][U_k S_l \circ I]}{[U_k S_l]},$$

$$[S_{k_2} \circ A_k S_l \circ I] \approx \frac{l-1}{l} \frac{[A_k S_l \circ S_{k_2}][A_k S_l \circ I]}{[A_k S_l]},$$

$$[S_{k_2} \circ P_k S_l \circ I] \approx \frac{l-1}{l} \frac{[P_k S_l \circ S_{k_2}][P_k S_l \circ I]}{[P_k S_l]},$$

$$[S_{k_2} \circ R_k S_l \circ I] \approx \frac{l-1}{l} \frac{[R_k S_l \circ S_{k_2}][R_k S_l \circ I]}{[R_k S_l]},$$

$$\begin{aligned}[S_{k_2} \circ S_l \circ I] = {} & [S_{k_2} \circ U S_l \circ I] + [S_{k_2} \circ A S_l \circ I] \\ & + [S_{k_2} \circ P S_l \circ I] + [S_{k_2} \circ R S_l \circ I].\end{aligned}$$

We expect the value of $\hat{\beta}_{l,\,k_2}$ in Eq. (4.5) to be smaller than its value in Eq. (4.4). This, in turn, leads to a smaller estimate of the disease prevalence from Eq. (4.5) than from Eq. (4.4). Intuitively, because individuals who hold the anti-physical-distancing opinion become infected at a higher rate, a typical susceptible individual is less likely to have an anti-physical-distancing opinion than a member of the population that one selects uniformly at random. Therefore, we expect that $[A] \geq \frac{[AS_l]}{[S_l]}$. By applying analogous reasoning to individuals who hold the pro-physical-distancing opinion, we expect that $[P] \leq \frac{[PS_l]}{[S_l]}$. We do not have a mathematically rigorous understanding of how well the approximations (4.5) and (4.6) match the

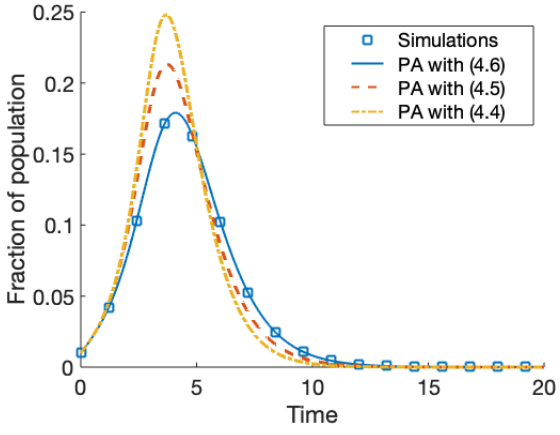

Fig. 5. (Color online) Comparison of our pair approximations (PAs) based on Eqs. (4.4)–(4.6) (the curves) with direct numerical simulations (the markers). The trajectories show the time evolution of the infectious population. In each simulation, we generate a network with layers that consist of 5-regular configuration-model graphs (i.e. each node has degree 5). We uniformly randomly infect a fraction $I_0 = 0.01$ of the nodes, and we independently and uniformly randomly choose initial opinions such that $A_0 = P_0 = 0.005$. The displayed results are means of 100 simulations. The other parameters are $\beta_{\text{phy}} = \beta_{\text{info}} = 0.6$, $\gamma_{\text{phy}} = \gamma_{\text{info}} = 1$, $\alpha_{\text{anti}} = 10$, and $\alpha_{\text{pro}} = 0.1$.

full stochastic system (see Sec. 2 and our code in Ref. 57). We compare the three different pair approximations of the disease prevalence that are based on Eqs. (4.4)–(4.6) with direct numerical simulations of the full stochastic system in Fig. 5. From this comparison, we see that the approximations (4.4) and (4.5) overestimate the infectious population and that the approximation (4.6) matches the simulations very well. These numerical results indicate that it is essential to track the coupling of the nodes' states at both ends of inter-layer edges and intra-layer edges to ensure accurate estimation of the time evolution of disease prevalence. We use the pair approximation (4.1, 4.2, 4.6) in our experiments in Sec. 5.

5. Computational Experiments

We now investigate our full model by simulating the stochastic system (see our code in Ref. 57) and applying the pair approximation (4.1, 4.2, 4.6), which we henceforth call our "PA". We explore the influence of competing opinion contagions on the spread of a disease for a variety of parameter values. We focus on examining different opinion contagion parameters (see Sec. 5.1) and network structures (see Secs. 5.2 and 5.3). For ease of comparison, we consider the special case in which the pro- and anti-physical-distancing opinions share the same contagion parameters for all examples in our paper. Additionally, we fix the disease contagion parameters to be $\beta_{\text{phy}} = 0.6$ and $\gamma_{\text{phy}} = 1$. Unless we specify otherwise, we set the opinion influence coefficients to be $\alpha_{\text{pro}} = 0.1$ and $\alpha_{\text{anti}} = 10$ to incorporate nontrivial influence of the corresponding opinion on the spread of the disease. This asymmetry between the pro- and anti-physical-distancing opinions affects the dynamics in an interesting way, as we illustrate in this section. In many of the following examples, it is helpful to separate the influence of the two opinions to gain understanding of the overall system behavior. To do this, we suppress the influence of an opinion by setting its influence coefficient to 1. In Sec. 5.1, we do a parameter sweep of the opinion transmission parameters in the range [0, 2] to illustrate that the final epidemic size can change non-monotonically as we increase the recovery rate of an opinion. This feature occurs in networks with a variety of degree distributions. Because of the issuing or lifting of stay-at-home orders, people's contact patterns in the offline world can change a lot over the course of an epidemic (and especially a pandemic).[20,76] In Secs. 5.2 and 5.3, we show examples that illustrate that the influence of an opinion contagion on the spread of a disease can change in important ways when we change the intra-layer or cross-layer correlations of intra-layer degrees.

In each computational experiment, we construct a network of $N = 10{,}000$ nodes and simulate the dynamics on it using a Gillespie algorithm,[42] which is a well-known approach for performing continuous-time simulations of Markovian processes. In all experiments in this section, we report results as means of 200 simulations. In each simulation, we generate a new random graph (of a few different types, which we specify below). We uniformly randomly infect $I_0 = 1\%$ of the nodes in the physical layer, and we independently and uniformly randomly choose $A_0 = P_0 = 0.5\%$ nodes

as anti- or pro-physical-distancing in the information layer. We set all remaining node states to S in the physical layer and to U in the information layer. Henceforth, unless we state otherwise, we use these choices of initial states in our numerical computations.

In our initial experiments, we construct each network layer from a configuration model[21] and match the nodes from the two layers uniformly at random. Specifically, we specify degree distributions $\mathbb{P}_{\text{info}}$ and $\mathbb{P}_{\text{phy}}$, which need not be the same. For each layer, we sample a degree sequence $\{k_i\}$ (where $i \in \{1, \dots, N\}$ indexes the nodes) from the corresponding degree distribution; therefore, node i has k_i ends of edges (i.e. stubs). We match these stubs uniformly at random to form a network. Correspondingly, in the pair approximation, we have

$$[Y_{k_1} X_{k_2}](0) = Y_0 X_0 \mathbb{P}_{\text{info}}(k_1) \mathbb{P}_{\text{phy}}(k_2)\,,$$

$$[Y_{k_1} X_{k_2} \circ Z_{k_3}](0) = \begin{cases} [Y_{k_1} X_{k_2}](0) \times Z_0 \mathbb{P}_{\text{info}}(k_3) k_1 k_3 / \langle k_{\text{info}} \rangle\,, & Z \in \{U,\, P,\, A,\, R_{\text{info}}\} \\ [Y_{k_1} X_{k_2}](0) \times Z_0 \mathbb{P}_{\text{phy}}(k_3) k_2 k_3 / \langle k_{\text{phy}} \rangle\,, & Z \in \{S,\, I,\, R_{\text{phy}}\}\,. \end{cases}$$

In Fig. 6, we compare typical disease prevalence curves (i.e. the time evolution of infectious populations) when we choose different coefficients for the influence of the opinions. The influence from the information layer changes a disease's prevalence, its peak value, and the time at which the peak number of infections occurs. Although an opinion does not alter the susceptibility of individuals to infection when the corresponding influence coefficient is 1, the spread of that opinion can still indirectly affect the overall disease dynamics, which thus can be different from the dynamics in a system with only one opinion. For example, in Fig. 6(a), the purple curve with triangle markers (for which $\alpha_{\text{anti}} = 1$ and $\alpha_{\text{pro}} = 0.1$) has a higher disease prevalence than the green curve with plus signs (for which $\alpha_{\text{pro}} = 0.1$ and the anti-physical-distancing opinion is absent). The spread of the anti-physical-distancing opinion prevents some people from adopting the pro-physical-distancing opinion, although the anti-physical-distancing opinion has an influence coefficient of 1. We show the dynamics on the information layer in Figs. 6(b) and 6(c).

5.1. *Opinion contagion parameters*

Recall from Sec. 3 that in a fully-mixed population with $\alpha_{\text{pro}} + \alpha_{\text{anti}} > 2$, the information layer leads to a larger epidemic size than when there is no influence from the information layer. We repeat the experiment in Fig. 4, but now we have a network structure and we employ our PA. We again consider the scenario in which the anti- and pro-physical-distancing opinions have the same contagion parameter values; we denote this situation using the subscript "info". Figure 7(a) shows final epidemic sizes versus the recovery rate γ_{info} in the information layer for the following three situations: (1) all nodes have degree 5 (i.e., we consider 5-regular graphs); (2) all node degrees follow a Poisson distribution with mean 5; and (3) all node degrees follow a truncated power-law distribution with $\mathbb{P}(k = x) \propto x^{-1.32} e^{-x/35}$ for $x \leq 50$

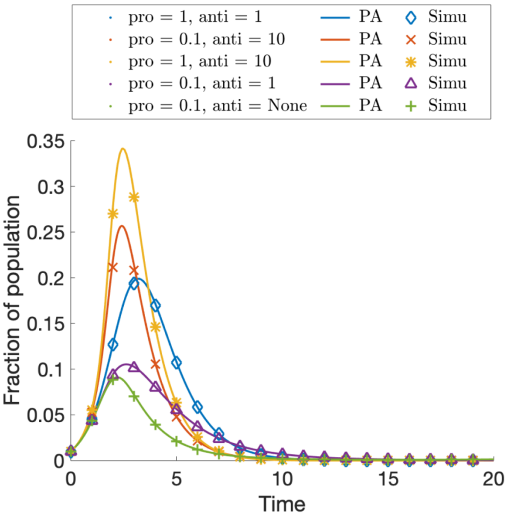

(a) Disease prevalence

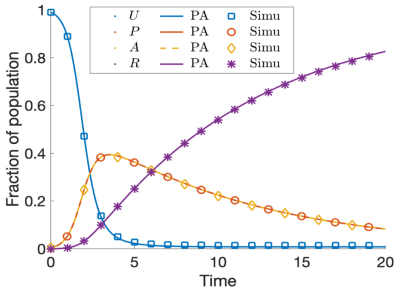

(b) Information layer; only the pro-physical-distancing opinion has influence

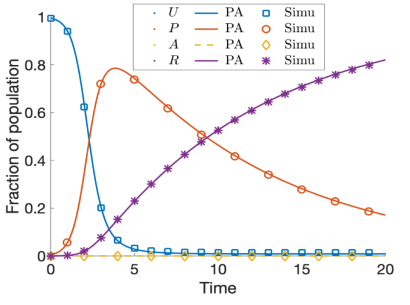

(c) Information layer; no anti-physical-distancing opinion

Fig. 6. (Color online) Dynamics for different opinion influence coefficients. (a) Disease prevalence curves for different influence coefficients, including when the anti-physical-distancing opinion is absent (which we denote by "anti = None"). In (b, c), we show the dynamics on the information layer when (b) both opinions are present and (c) only the pro-physical-distancing opinion is present. We construct each layer from a configuration model with a degree sequence that we choose from a Poisson degree distribution with mean degree 5. The other parameters are $\beta_{\text{phy}} = \beta_{\text{info}} = 0.6$, $\gamma_{\text{phy}} = 1$, and $\gamma_{\text{info}} = 0.1$. The curves (respectively, markers) indicate results from the PA (respectively, from means of 200 direct simulations).

and $\mathbb{P}(k = x) = 0$ for $x > 50$. In each situation, we generate both layers using configuration-model networks and we independently sample degrees for each layer from the same distribution. The mean degree is roughly 5 in all three situations. In all three situations, the final epidemic size can be smaller than the corresponding basic size (i.e. without opinion spread) when γ_{info} is very small. As we increase γ_{info}, the final epidemic size first increases and surpasses the basic size before reaching a peak; it subsequently decreases to the basic size.

To explain this non-monotonic behavior, we decompose the recovered population at steady state into subpopulations based on their opinion states when they become infectious and plot the relative size of each subpopulation (with a sum that is normalized to 1) in Fig. 7(b). We use $\mathcal{U}$, $\mathcal{A}$, $\mathcal{P}$, and $\mathcal{R}$ to denote the subpopulations that become infectious when they are in the U, A, P, and R_{info} states, respectively. We show results when both layers are 5-regular graphs. Our results on

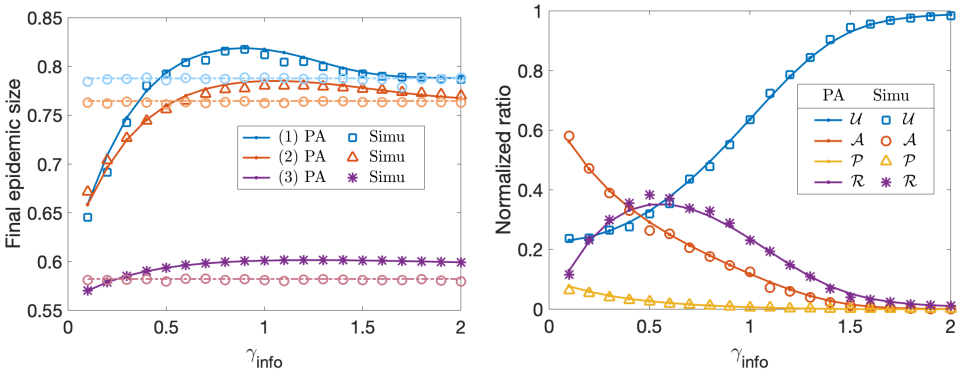

(a) Final epidemic size (b) Decomposition of opinion states

Fig. 7. (Color online) Influence of the opinion recovery rate γ_{info} on disease prevalence and on the distribution of opinion states when nodes become infectious. (a) The final epidemic size for different values of γ_{info}. The solid curves and non-circle symbols mark the final epidemic sizes when there is influence from the information layer. The dashed curves and circles mark the basic size. We consider three situations: (1) each layer is a 5-regular graph; (2) all node degrees follow a Poisson distribution with mean 5; and (3) all node degrees follow a truncated power-law distribution with $\mathbb{P}(k = x) \propto x^{-1.32}e^{-x/35}$ for $x \leq 50$ and $\mathbb{P}(k = x) = 0$ for $x > 50$. We construct each layer from a configuration model with a degree sequence from the specified degree distribution. The other parameters are $\beta_{\text{phy}} = \beta_{\text{info}} = 0.6$, $\gamma_{\text{phy}} = 1$, $\alpha_{\text{anti}} = 10$, and $\alpha_{\text{pro}} = 0.1$. (b) We group recovered nodes based on their opinion states when they become infectious (we use the notation $\mathcal{U}$, $\mathcal{P}$, $\mathcal{A}$, and $\mathcal{R}$ for these subpopulations) and plot the normalized size. We show results for 5-regular configuration-model graphs. The curves (respectively, markers) indicate results from the PA (respectively, from means of 200 direct simulations).

networks with the Poisson and truncated power-law distribution are qualitatively the same. Because increasing opinion recovery rates results in fewer people adopting any opinion, the size of the $\mathcal{U}$ subpopulation increases (i.e. more people become infected while uninformed). For the same reason, the sizes of the subpopulations with the anti- and pro-physical-distancing opinions decrease with increasing opinion recovery rates. The size of the $\mathcal{R}$ subpopulation first increases as we increase γ_{info}. This occurs because when γ_{info} is very small, many people keep the same opinion (P or A) until the disease dies out in the population. When we start to increase γ_{info}, more people recover from an opinion when the disease is still actively spreading. Because people who abandon the pro-physical-distancing opinion increase their risk of becoming infected, the overall epidemic size may increase when they become less cautious. As γ_{info} grows, fewer nodes adopt an opinion; this, in turn, leads to a smaller $\mathcal{R}$ subpopulation and a drop in the overall epidemic size.

The non-monotonic behavior that we described above suggests that if enough people hold the pro-physical-distancing opinion for a sufficiently long time, the prevalence of a disease can decrease, even when the anti-physical-distancing opinion has an arbitrarily large influence coefficient. When both opinions are present, the overall influence of opinions on disease spread is not determined by the two influence coefficients alone; instead, it arises from a complex interaction between the dynamics of the two opinions.

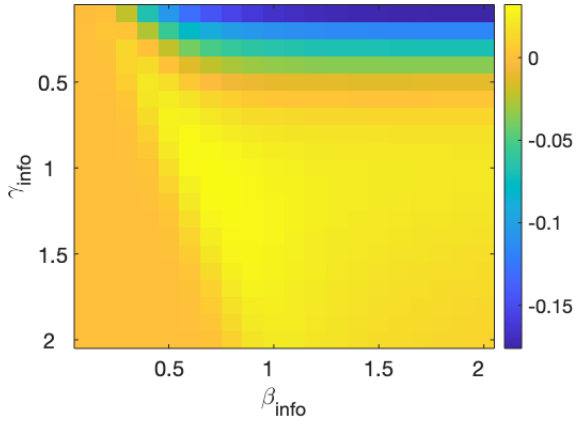

Fig. 8. (Color online) The final epidemic size minus the basic size for different values of the opinion contagion parameters for our PA on networks with layers that consist of 5-regular configuration-model graphs. We fix the other parameters to be $\beta_{\text{phy}} = 0.6$, $\gamma_{\text{phy}} = 1$, $\alpha_{\text{anti}} = 10$, and $\alpha_{\text{pro}} = 0.1$.

We plot the final epidemic size minus the basic size in Fig. 8 for different values of the opinion transmission rates and opinion recovery rates. For fixed opinion recovery rates, the final epidemic size does not change much as we vary the opinion transmission rates if the information layer has an outbreak. The results in Fig. 8 are outputs of our PA on 5-regular configuration-model graphs.

5.2. *Random graphs with intra-layer degree–degree correlations*

Many nodes in a network having intra-layer edges to other nodes of similar degrees (i.e. the network is assortative by degree,[52,54] which is often called simply "assortative") can have a strong impact on disease spread and other dynamical processes.[41,48] Such assortative networks may have a core with large-degree nodes, so a disease may spread faster but terminate with a smaller final epidemic size on such a network than on a disassortative network.[51,54] In this subsection, we investigate how differences in assortativity structure, which we encode in an intra-layer degree–degree correlation matrix, can influence the dynamics of our model.

For all experiments in this subsection, we generate networks with intra-layer degree–degree correlations using a model from Melnik *et al.*[48] For each of the two layers in the network, we start with a mixing matrix E that specifies the joint distribution of degrees at both ends of an edge that we choose uniformly at random. The number of edges that connect nodes with degrees k and k' is $\mathcal{E}_{k,k'} = E_{k,k'} \sum_k (kp_k)N/2$, where $p_k = \left(\sum_{k'} \frac{E_{k,k'}}{k}\right) / \left(\sum_{k,k'} \frac{E_{k,k'}}{k}\right)$ specifies the degree distribution and we recall that N is the number of nodes. We first create the required number of edges that will connect node pairs with specified combinations of the degrees k and k'. We then generate nodes by selecting k ends of edges uniformly at random from those that are prescribed to attach to degree-k nodes. We obtain

networks with the desired degree–degree correlation when we finish attaching all ends of edges to nodes.

Because we track the expected number of edges with all possible degree combinations explicitly and separately in the PA system, we only need to modify the initialization step to encode the desired intra-layer degree–degree correlation. For example, we let $[U_k \circ P_l](0) = \mathcal{E}_{\text{info},\,k,\,l} \times (1 - P_0 - A_0)P_0$, where $\mathcal{E}_{\text{info},\,k,\,l}$ denotes the number of edges that connect degree-k and degree-l nodes in the information layer. We initialize the physical layer and the information layer independently, so $[U_{k_1} S_{k_2} \circ P_l](0) = [U_{k_1} \circ P_l](0) \times \mathbb{P}_{\text{phy}}(k_2) \times (1 - I_0)$. We initialize the other dyads similarly.

5.2.1. *Pedagogical example*: *Networks whose nodes have one of two different degrees*

To illustrate the importance of intra-layer degree–degree correlations, we consider a simple example of a network whose nodes have one of two different degrees. Its degree distribution is $\mathbb{P}(k = k_1) = p_1$ and $\mathbb{P}(k = k_2) = p_2$, where $p_1 + p_2 = 1$. The mixing matrix is

$$E = \begin{bmatrix} a & \dfrac{k_1 p_1}{\langle k \rangle} - a \\ \dfrac{k_1 p_1}{\langle k \rangle} - a & \dfrac{k_2 p_2 - k_1 p_1}{\langle k \rangle} + a \end{bmatrix}, \tag{5.1}$$

where $a \in \left[\max\left\{0, \frac{k_1 p_1 - k_2 p_2}{\langle k \rangle}\right\}, \frac{k_1 p_1}{\langle k \rangle}\right]$ and $\langle k \rangle$ denotes the mean degree. We calculate the assortativity coefficient r_{intra}, which is given by the Pearson correlation coefficient of the degrees at the two ends of an edge that we choose uniformly at random. Given the mixing matrix (5.1), the assortativity coefficient r_{intra} is linear in a and is given by

$$r_{\text{intra}} = \frac{a - k_1^2 p_1^2 / \langle k \rangle^2}{k_1 k_2 p_1 p_2 / \langle k \rangle^2}.$$

Figure 9 shows two typical sets of curves for the final epidemic size for different values of the intra-layer degree–degree correlation. We fix $k_1 = 2$ and $k_2 = 8$, and we assign 40% of the nodes to have degree 2 in Fig. 9(a) and 90% of them to have degree 2 in Fig. 9(b). We set the intra-layer degree–degree correlations to be the same in the two layers. The blue circles indicate the influence of degree assortativity on disease spreading when the disease spreads independently of opinions. The decreasing trend in Fig. 9(a) and in the right part of Fig. 9(b) is consistent with the known result[41,51] that a disease tends to affect a smaller fraction of a population in an assortative network than in a disassortative network when an epidemic outbreak occurs. The increasing trend in the left part of Fig. 9(b) arises from the fact that the disease is initially impeded from spreading because of the disassortative structure and a denser network helps the disease to spread and persist. Similar trends also occur in

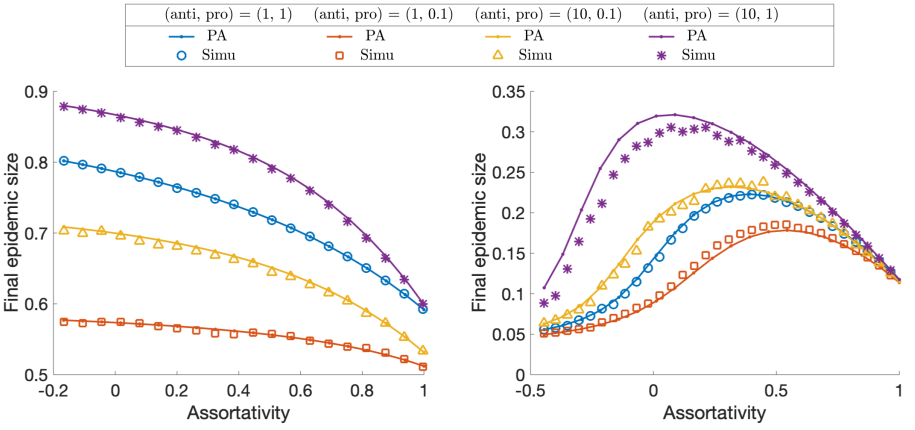

(a) $\mathbb{P}_{\text{info}}(k=2) = \mathbb{P}_{\text{phy}}(k=2) = 0.4$ (b) $\mathbb{P}_{\text{info}}(k=2) = \mathbb{P}_{\text{phy}}(k=2) = 0.9$

Fig. 9. (Color online) The final epidemic size depends on the intra-layer degree–degree correlations. We generate each layer independently using a generalization of a configuration-model network with the procedure that we described in the text. Each layer consists of nodes with degrees 2 and 8, and the intra-layer degree–degree correlation is the same in the two layers. The other parameters are $\beta_{\text{phy}} = \beta_{\text{info}} = 0.6$, $\gamma_{\text{phy}} = 1$, and $\gamma_{\text{info}} = 0.1$. The curves (respectively, markers) indicate results from our PA (respectively, from means of 200 direct simulations).

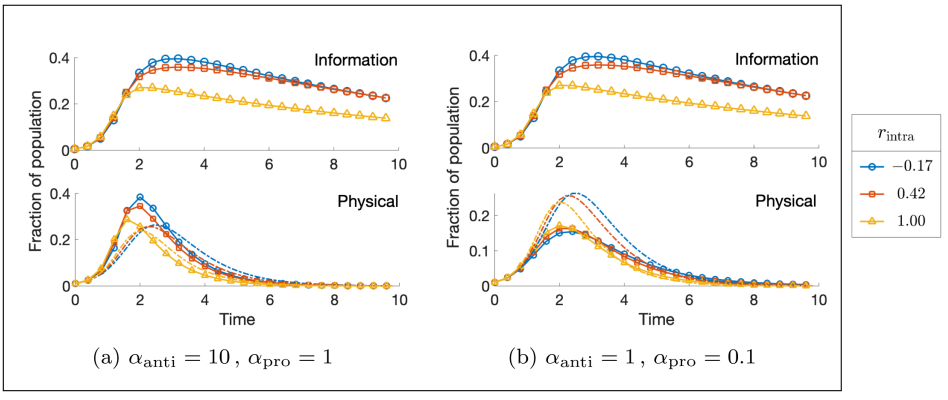

(a) $\alpha_{\text{anti}} = 10$, $\alpha_{\text{pro}} = 1$ (b) $\alpha_{\text{anti}} = 1$, $\alpha_{\text{pro}} = 0.1$

Fig. 10. (Color online) Prevalence curves from our PA for different intra-layer degree–degree correlations in networks with $\mathbb{P}_{\text{info}}(k=2) = \mathbb{P}_{\text{phy}}(k=2) = 0.4$ and $\mathbb{P}_{\text{info}}(k=8) = \mathbb{P}_{\text{phy}}(k=8) = 0.6$. We generate each layer independently using a generalization of a configuration-model network with the procedure that we described in the text. The upper row shows the (identical) dynamics of the fraction of individuals in the P and A states. The lower row shows the dynamics of the population in the I state. The solid curves show results when (left) $\alpha_{\text{anti}} = 10$ and $\alpha_{\text{pro}} = 1$ and (right) $\alpha_{\text{anti}} = 1$ and $\alpha_{\text{pro}} = 0.1$. The dashed curves indicate results without any opinion contagion. The other parameters are $\beta_{\text{phy}} = \beta_{\text{info}} = 0.6$, $\gamma_{\text{phy}} = 1$, and $\gamma_{\text{info}} = 0.1$. Curves with the same color share all parameters except opinion influence coefficients.

the information layer, so if outbreaks do occur on both layers, an opinion contagion has a smaller impact when networks have a larger degree assortativity (as we see in both panels of Fig. 9). In Fig. 10, we compare the disease prevalence curves with and without the influence of each opinion for networks with $\mathbb{P}_{\text{info}}(k = 2) = \mathbb{P}_{\text{phy}}(k = 2) = 0.4$. The results demonstrate that disassortative structures tend to enhance the influence of both the pro- and anti-physical-distancing opinions. When both opinions have nontrivial effects on the transmission of a disease, the overall effect of the opinion dynamics on the disease dynamics is a complicated combination of the dynamics of the opinions; in this situation, it is unclear whether an assortative or a disassortative structure promotes the spread of the disease.

The intra-layer degree–degree correlations in the two layers need not be the same. Figure 11 shows heat maps of the final epidemic size from our PA for different values of the two degree–degree correlations, which we vary independently in each layer. The issuance of a stay-at-home order may lead to a physical layer with many small-degree nodes, and such an order is not likely to affect the information layer (which may describe online contacts). Therefore, we also consider the case with $\mathbb{P}_{\text{info}}(k = 2) = 0.4$ and $\mathbb{P}_{\text{phy}}(k = 2) = 0.9$. We show the results for this case in the third row of Fig. 11. In this example, the physical-layer network structures have a stronger influence on the disease dynamics than the information-layer network structures.

5.3. *Random graphs with cross-layer correlations of intra-layer degrees*

We also investigate the influence of cross-layer correlations of intra-layer degrees on the dynamics. We refer to such correlations as "inter-layer degree–degree correlations". People who are active on social-media platforms may also have frequent offline social contacts, and vice versa.[1] Let C denote the inter-layer degree–degree correlation matrix, so $C_{k_1,\,k_2}$ is the probability that a node that we choose uniformly at random has degree k_1 in the information layer and degree k_2 in the physical layer. We say that these nodes are "of type $(k_1,\,k_2)$". An uncorrelated model corresponds to $C_{k_1,\,k_2} = \mathbb{P}_{\text{info}}(k_1)\mathbb{P}_{\text{phy}}(k_2)$. We uniformly randomly pair $N \times C_{k_1,\,k_2}$ degree-k_1 nodes from the information layer with the same number of degree-k_2 nodes from the physical layer to construct a network with N nodes and a specified inter-layer degree–degree correlation.

As with the situation in Sec. 5.2, a PA can deal with inter-layer degree–degree correlations properly as long as we build them into the initial conditions. The modification of the PA is straightforward. For example, we write

$$[U_{k_1} S_{k_2}](0) = C_{k_1\,k_2}(1 - A_0 - P_0)(1 - I_0)\,,$$

$$[U_{k_1} S_{k_2} \circ I_l](0) = [S_{k_2} \circ I_l](0) \times \frac{C_{k_1\,k_2}}{\mathbb{P}_{\text{phy}}(k_2)} \times (1 - A_0 - P_0)\,.$$

We use similar formulas for the other pairs.

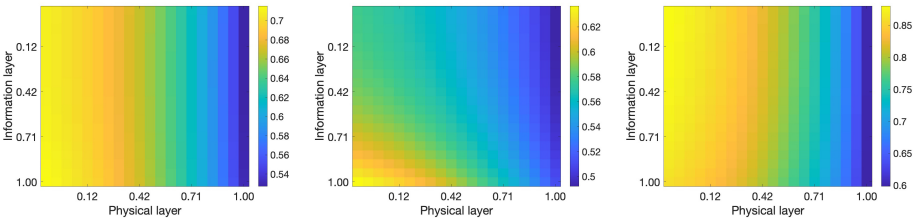

(a) $\mathbb{P}_{\text{info}}(k=2) = \mathbb{P}_{\text{phy}}(k=2) = 0.4$

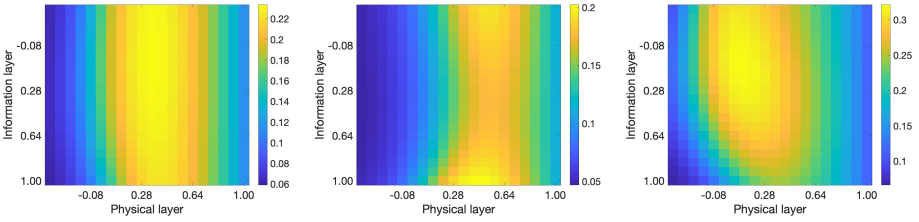

(b) $\mathbb{P}_{\text{info}}(k=2) = \mathbb{P}_{\text{phy}}(k=2) = 0.9$

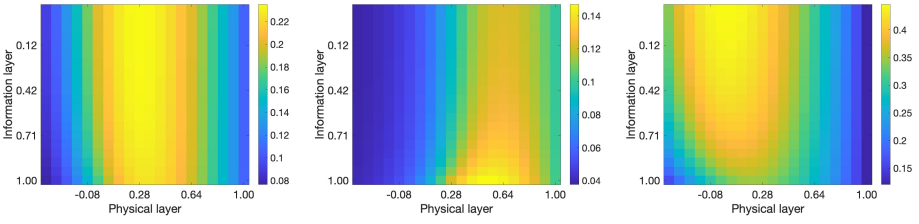

(c) $\mathbb{P}_{\text{info}}(k=2) = 0.4$, $\mathbb{P}_{\text{phy}}(k=2) = 0.9$

Fig. 11. (Color online) Heat maps of the final epidemic size from our PA as we vary the assortativities in the two layers. The three columns have parameter values of (left) $\alpha_{\text{pro}} = 0.1$ and $\alpha_{\text{anti}} = 10$, (center) $\alpha_{\text{pro}} = 0.1$ and $\alpha_{\text{anti}} = 1$, and (right) $\alpha_{\text{pro}} = 1$, and $\alpha_{\text{anti}} = 10$. The other parameters are $\beta_{\text{phy}} = \beta_{\text{info}} = 0.6$, $\gamma_{\text{phy}} = 1$, and $\gamma_{\text{info}} = 0.1$.

5.3.1. *Pedagogical example*: *Networks whose nodes have one of two different degrees*

We again suppose that nodes have one of two different degrees in each layer. These degrees are $k_{\text{info},1}$, $k_{\text{info},2}$, $k_{\text{phy},1}$, and $k_{\text{phy},2}$, where $\mathbb{P}_{\text{info}}(k = k_{\text{info},1}) = q_1$ and $\mathbb{P}_{\text{phy}}(k = k_{\text{phy},1}) = q_2$. The correlation matrix C is

$$\begin{bmatrix} a & q_1 - a \\ q_2 - a & 1 - q_1 - q_2 + a \end{bmatrix}, \tag{5.2}$$

where $a \in [\min\{0,\, q_1 + q_2 - 1\},\, \min\{q_1,\, q_2\}]$. The Pearson correlation coefficient is

$$r_{\text{inter}} = \frac{(k_{\text{info},1} - k_{\text{info},2})(k_{\text{phy},1} - k_{\text{phy},2})(a - q_1 q_2)}{\sigma_{\text{info}} \sigma_{\text{phy}}},$$

where σ_{info} and σ_{phy} denote the standard deviations of the degrees in the two layers.

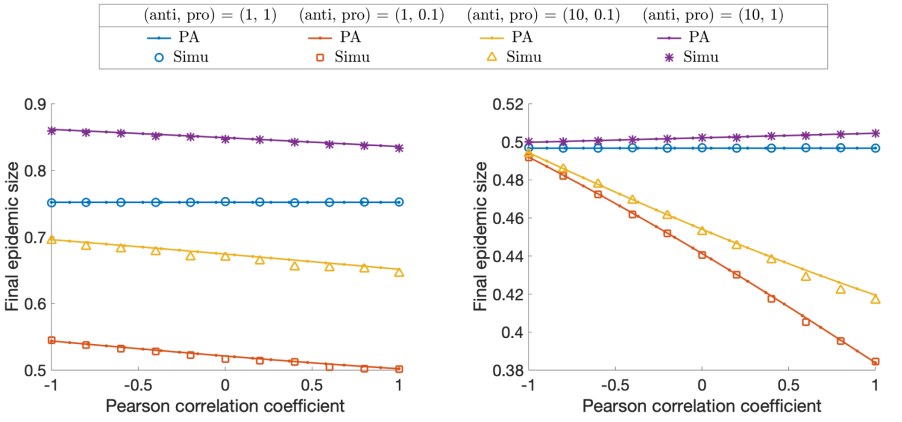

(a) $r_{\text{intra}} = -0.25$ (b) $r_{\text{intra}} = 1$

Fig. 12. (Color online) The final epidemic size depends on the inter-layer degree–degree correlation. Both layers have nodes of degrees 2 and 8, and we set $\mathbb{P}_{\text{info}}(k = 2) = \mathbb{P}_{\text{phy}}(k = 2) = 0.5$. We generate each layer using the procedure in Sec. 5.2. We couple the two layers following the approach in Sec. 5.3. We set the intra-layer degree–degree correlation of both layers to be (a) -0.25 and (b) 1. The other parameters are $\beta_{\text{phy}} = \beta_{\text{info}} = 0.6$, $\gamma_{\text{phy}} = 1$, and $\gamma_{\text{info}} = 0.1$. The curves (respectively, markers) show results from our PA (respectively, from means of 200 direct simulations).

Figure 12 shows the dependence of the final epidemic size on the inter-layer degree–degree correlations. Each of the two layers has nodes of degrees 2 and 8, and we set $\mathbb{P}_{\text{info}}(k = 2) = \mathbb{P}_{\text{phy}}(k = 2) = 0.5$. We generate each layer independently with a generalization of a configuration-model network following the procedure in Sec. 5.2. We suppose either that both intra-layer degree–degree correlations are -0.25 or that both intra-layer degree–degree correlations are 1, and we couple the two layers as described above.[a] The pro-physical-distancing opinion has a larger influence when the two layers are more positively correlated. (See the red curves with square markers.) However, the anti-physical-distancing opinion's influence can either decrease or increase as we increase the inter-layer degree–degree correlation. (See the purple curves with asterisk markers.)

To understand the trends in Fig. 12, we again decompose the population based on their opinion states (see Fig. 13). Recall that $\mathcal{U}$, $\mathcal{A}$, $\mathcal{P}$, and $\mathcal{R}$ denote the subpopulations that become infectious when they are in the U, A, P, and R_{info} states, respectively. Additionally, we decompose the $\mathcal{U}$ and $\mathcal{A}$ subpopulations based on node degrees and plot the fraction of the population in each group in Fig. 14. We examine the effects of negative intra-layer degree–degree correlations in Figs. 13(a) and 14(a,c), and we examine the effects of positive intra-layer degree–degree correlations (which we will discuss first) in Figs. 13(b) and 14(b,d). In our discussion, it is instructive to consider the case of two independent layers (i.e. $\alpha_{\text{pro}} = \alpha_{\text{anti}} = 1$).

[a]A layer with an intralayer degree–degree correlation of 1 has more than one component.

The inter-layer degree–degree correlation changes the opinion distributions, but the final epidemic size stays the same. We investigate the influence of opinions and how such influence depends on the inter-layer degree–degree correlation.

We first examine the case in which the intra-layer degree–degree correlation is 1 and node opinions do not affect the spread of the disease. A positive inter-layer degree–degree correlation encourages the coupling of large-degree nodes in the two layers; these nodes have larger probabilities than small-degree nodes both of becoming infected and of forming an opinion. Therefore, as we increase the inter-layer degree–degree correlation, fewer nodes are uninformed when they catch the disease. Figure 14(b) shows the decomposition of the $\mathcal{U}$ subpopulation based on the degrees of its nodes. Because the degree-2 nodes are adjacent only to other degree-2 nodes in each layer, they are rarely infectious and rarely form an opinion. Therefore, the $\mathcal{U}$ subpopulation consists primarily of nodes of types (2, 8) and (8, 8). As we increase the inter-layer degree–degree correlation, there are more (8, 8)-type nodes and fewer (2, 8)-type nodes in the network. Because U_8-nodes (i.e. nodes that are uninformed and have degree 8 in the information layer) have a larger probability of forming an opinion than U_2-nodes, fewer nodes become infected while still uninformed as we increase the correlation.

If we perturb the influence coefficients α_{anti} and α_{pro} from 1, the opinions on the information layer directly affect the $\mathcal{A}$ and $\mathcal{P}$ subpopulations, respectively, through modified infection risks. These modified risks then influence the speed of disease spread and affect the other subpopulations. Therefore, the information layer has a larger effect on the disease dynamics when more people become infected while holding some opinion. Based on our discussion above, we expect that increasing the inter-layer degree–degree correlation amplifies the influence of opinion spread on disease dynamics.

We now examine the case in which either the pro-physical-distancing opinion or the anti-physical-distancing opinion has a nontrivial influence on disease dynamics. For simplicity, we suppose that only one opinion is effective. When $\alpha_{\text{pro}} < 1$, the spread of the pro-physical-distancing opinion protects people who adopt that opinion because it suppresses the spread of the disease. In Fig. 13(b), we see that the $\mathcal{U}$ subpopulation tends to decrease faster and that the $\mathcal{P}$ and $\mathcal{A}$ subpopulations tend to increase slower in this situation than when the disease spreads independently of opinions. Therefore, the final epidemic size decreases as we increase the inter-layer degree–degree correlation. When $\alpha_{\text{anti}} > 1$, the anti-physical-distancing opinion accelerates the spread of the disease. Therefore, more people become infected before their opinions change; this, in turn, leads to a larger $\mathcal{U}$ subpopulation and smaller $\mathcal{A}$, $\mathcal{P}$, and $\mathcal{R}$ subpopulations. The growing gap between the dashed purple curve and the dashed blue curve (i.e. between the $\mathcal{U}$ subpopulations for different parameter values) in Fig. 13(b) illustrates the increase in the epidemic size as we increase the inter-layer degree–degree correlation.

The situation is more intricate when the intra-layer degree–degree correlation is -0.25 in each layer. Because the intra-layer edges now can connect degree-2

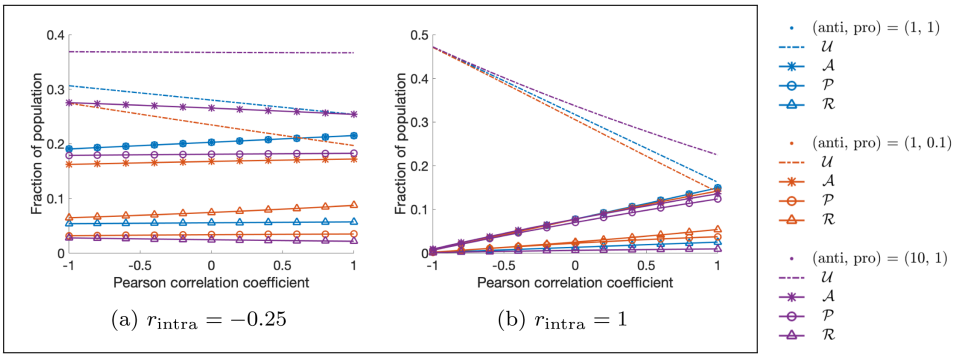

Fig. 13. (Color online) Decomposition of the opinion states of nodes that eventually become infectious and recover. We group the recovered population based on their opinion states when they become infectious. Recall that the associated subpopulations are $\mathcal{U}$, $\mathcal{P}$, $\mathcal{A}$, and $\mathcal{R}$. The vertical axis indicates the fraction of the population in each of these subpopulations. We plot the subpopulation sizes versus the inter-layer degree–degree correlation from our PA. The intra-layer degree–degree correlation is (a) -0.25 and (b) 1. The other parameters are $\beta_{\text{phy}} = \beta_{\text{info}} = 0.6$, $\gamma_{\text{phy}} = 1$, and $\gamma_{\text{info}} = 0.1$.

nodes to degree-8 nodes, the former are more likely both to become infectious and to adopt an opinion than when the intra-layer degree–degree correlations are 1. Therefore, when $\alpha_{\text{anti}} = \alpha_{\text{pro}} = 1$, nodes of types (8, 2) and (2, 2) constitute a larger proportion of the $\mathcal{U}$ subpopulation in Fig. 14(a) than in Fig. 14(b). As we increase the inter-layer degree–degree correlation, the $\mathcal{U}$ subpopulation has progressively more nodes with degree 2 in the physical layer because there are gradually fewer (8, 2)-type nodes and gradually more (2, 2)-type nodes and it is more difficult for the (2, 2)-type nodes to form an opinion. Consequently, the decreasing trend in the $\mathcal{U}$ subpopulation (see the dashed blue curve) in Fig. 13(a) is less drastic than in Fig. 13(b).

When $\alpha_{\text{anti}} > 1$, the $\mathcal{A}$ subpopulation in Fig. 13(a) (see the purple curve with asterisk markers) has qualitatively different dynamics than in Fig. 13(b). This difference arises from the influence of opinions on degree-2 nodes in the physical layer. Nodes that adopt the anti-physical-distancing opinion now have a larger infection risk than when $\alpha_{\text{anti}} = 1$, so we expect more nodes to become infected while holding the anti-physical-distancing opinion. In Fig. 14(c), we see that the anti-physical-distancing opinion leads to an increase in the numbers of nodes of types (8, 2) and (2, 2) in the $\mathcal{A}$ subpopulation as we increase α_{anti} from 1 to 10. Moreover, as we increase α_{anti} from 1 to 10, the increase in the number of (8, 2)-type nodes in the $\mathcal{A}$ subpopulation when the inter-layer degree–degree correlation is -1 is larger than the increase in the number of (2, 2)-type nodes in that subpopulation when the inter-layer degree–degree correlation is 1. This phenomenon arises because degree-8 nodes are more likely than degree-2 nodes to adopt an opinion. This, in turn, leads to a decrease of the $\mathcal{A}$ subpopulation and ultimately to a decrease of the total epidemic size as we increase the inter-layer degree–degree correlation. The

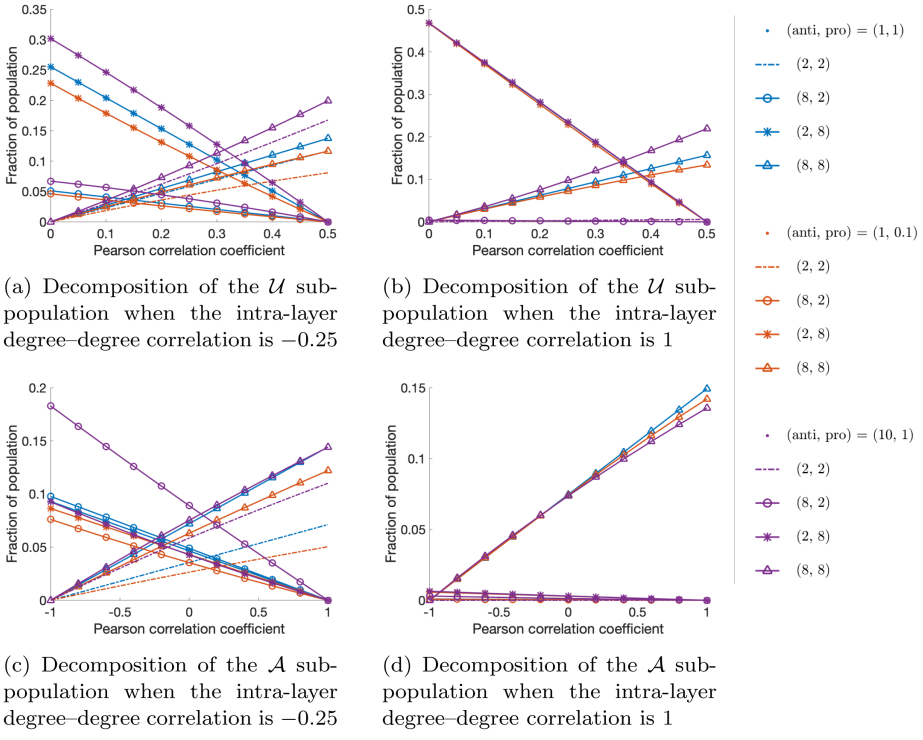

(a) Decomposition of the $\mathcal{U}$ subpopulation when the intra-layer degree–degree correlation is -0.25

(b) Decomposition of the $\mathcal{U}$ subpopulation when the intra-layer degree–degree correlation is 1

(c) Decomposition of the $\mathcal{A}$ subpopulation when the intra-layer degree–degree correlation is -0.25

(d) Decomposition of the $\mathcal{A}$ subpopulation when the intra-layer degree–degree correlation is 1

Fig. 14. (Color online) Decomposition based on the degrees of the nodes that eventually become infectious and recover. We decompose (a, b) the $\mathcal{U}$ subpopulation and (c, d) the $\mathcal{A}$ subpopulation by degree. The vertical axes indicate the fraction of the population in each subpopulation. We show the changes in subpopulation size versus the inter-layer degree–degree correlation from our PA. The other parameters are $\beta_{\text{phy}} = \beta_{\text{info}} = 0.6$, $\gamma_{\text{phy}} = 1$, and $\gamma_{\text{info}} = 0.1$.

anti-physical-distancing opinion does not lead to a clear increase in the number of degree-8 nodes in the $\mathcal{A}$ subpopulation. One plausible explanation is that the degree-8 nodes are already very likely to become infected at the baseline transmission rate of the disease. Additionally, the anti-physical-distancing opinion does not lead to an increase in the numbers of nodes of types (8, 2) or (2, 2) when the intra-layer degree–degree correlation is 1 (see Fig. 14(d)). We conjecture that this is because the positive intra-layer degree–degree correlation imposes sufficiently strong constraints so that it is difficult for nodes with degree 2 in the physical layer to become infected even when the transmission rate is high.

6. Modeling Temporary Immunity to Opinions

In previous sections, we assumed that people who adopt a pro- or anti-physical-distancing opinion develop immunity to both opinions after they recover. More generally, the opinions of individuals can change back and forth.[27] In this section, we extend the opinion dynamics to an SIRS process (see Fig. 15). With conversion

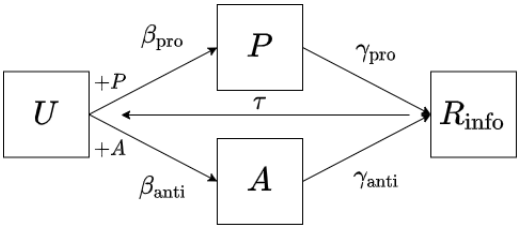

Fig. 15. Schematic illustration of the dynamics on the information layer with temporary immunity to opinions. The transitions are the same as in Fig. 1, except that nodes in state R_{info} transition to state U at rate τ.

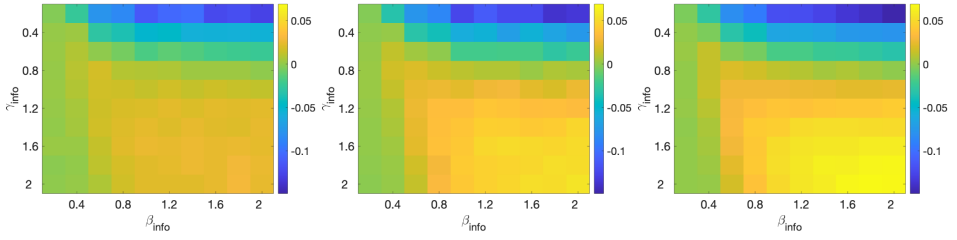

(a) $\tau = 0$ (b) $\tau = 1$ (c) $\tau = 2$

Fig. 16. (Color online) The final epidemic size minus the basic size as we vary γ_{info}, β_{info}, and τ in direct simulations of our refined model. We generate each layer using a configuration-model network with a Poisson degree distribution with a mean degree of 5. The other parameters are $\beta_{\text{phy}} = 0.6$, $\gamma_{\text{phy}} = 1$, $\alpha_{\text{anti}} = 10$, and $\alpha_{\text{pro}} = 0.1$. Each panel is a mean of 600 simulations.

rate τ, nodes in the R_{info} compartment return to the U compartment and again become susceptible to the pro- and anti-physical-distancing opinions. When $\tau = 0$, this refined model reduces to the model in Sec. 2 (see Fig. 1).

Figure 16 shows the final epidemic size minus the basic size as we vary the contagion parameters τ, γ_{info}, and β_{info} in direct simulations of our refined model. For a fixed value of τ, we obtain a heat map that is similar to the one in Fig. 8. As we increase τ, our simulations suggest that the overall influence from the information layer increases. For fixed values of γ_{info} and β_{info}, the colors in the heat map become brighter (respectively, darker) from left to right because the spread of opinions leads to a decrease (respectively, increase) in the final epidemic size in comparison to the basic size as we increase τ.

Consider the case $\beta_{\text{info}} = 2$, where the effect of τ is particularly evident. Figure 17(a) shows the influence of τ on the final epidemic size for a few values of γ_{info}. It is hard to see the trend when $\gamma_{\text{info}} = 1$ because of the stochasticity of the simulations, but the behavior of the other three curves is consistent with that of Fig. 16. As we increase τ, the expected duration that individuals stay in the R_{info} state decreases. Consequently, as we increase τ in Fig. 17(b), the size of the $\mathcal{R}$ subpopulation decreases and sizes of the other subpopulations ($\mathcal{U}$, $\mathcal{A}$, and $\mathcal{P}$) increase.

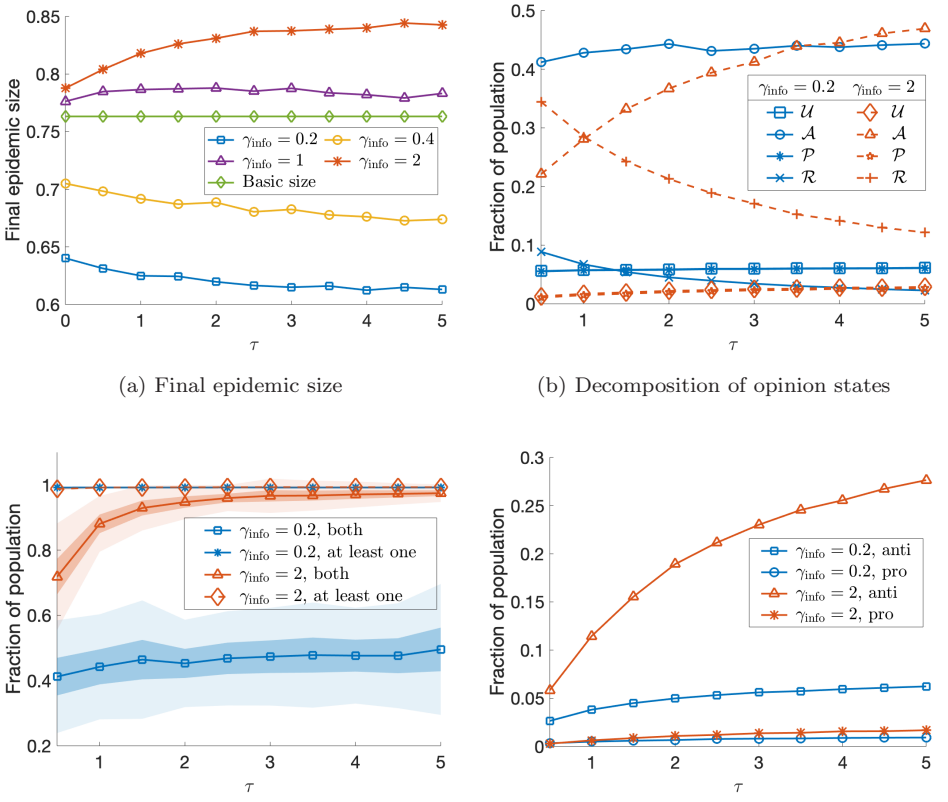

(a) Final epidemic size

(b) Decomposition of opinion states

(c) Fractions of the population that adopt (i) both opinions and (ii) at least one opinion

(d) Fractions of the population that are infected during their second or subsequent time that they adopt an opinion (the second and subsequent opinions need not be the same as prior opinions)

Fig. 17. (Color online) Influence of the opinion recovery rate γ_{info} and the conversion rate τ on the final epidemic size and on the opinion distribution when we consider SIRS dynamics in the information layer. (a) The influence of τ on the final epidemic size. We decompose the recovered population based on their opinion states when they become infected and plot the sizes of these subpopulations in (b). In (c, d), we show additional opinion-distribution statistics; we specify them in the subtitles. We generate each layer using a configuration model with a Poisson degree distribution with a mean degree of 5. The curves show means of 200 direct simulations with $\beta_{\text{phy}} = 0.6$, $\gamma_{\text{phy}} = 1$, $\beta_{\text{info}} = 2$, $\alpha_{\text{pro}} = 0.1$, and $\alpha_{\text{anti}} = 10$.

We conjecture that the overall influence (i.e. whether increasing τ leads to more or fewer disease infections) depends on whether people tend to adopt an opinion that departs from their earlier opinion(s). If individuals tend to adopt different opinions over time, increasing τ makes the model with SIRS opinion dynamics exhibit behavior that resembles what we observed after applying the random-recoupling assumption (see Sec. 3) and leads to more people adopting the anti-physical-distancing opinion at an earlier time. Susceptible individuals are likely to become infected when

they adopt the anti-physical-distancing opinion, regardless of whether or not they have previously adopted the pro-physical-distancing opinion. Consequently, increasing τ leads to more disease infections. However, if people tend to adopt the same opinion over time, susceptible individuals who adopt the pro-physical-distancing opinion also are more likely to avoid future infections. In this case, enforcing a faster reversion to the U state has a similar effect as decreasing γ_{info}, which (as we showed in Sec. 5.1) may help suppress disease spreading. Figure 17(c) shows the fractions of individuals who adopt (i) both opinions and (ii) at least one opinion within the time frame of our experiments for $\gamma_{\text{info}} = 0.2$ and $\gamma_{\text{info}} = 2$. Many fewer people adopt both opinions when $\gamma_{\text{info}} = 0.2$ than when $\gamma_{\text{info}} = 2$. Additionally, as we increase τ, there is only a slightly increasing trend in the fraction of people who adopt both opinions for $\gamma_{\text{info}} = 0.2$, in contrast to the rapid growth of the fraction for $\gamma_{\text{info}} = 2$. Intuitively, a node that adopts one opinion can influence more neighbors when γ_{info} is smaller. Therefore, it is more likely to adopt the same opinion later. Suppose that a node holds an opinion when it becomes infected on the physical layer, and suppose that this is not the first opinion that it has held (i.e. it previously returned to the U state in the information layer). In Fig. 17(d), we examine the counts of these individuals for both opinions as a function of τ. Consistent with our conjecture, as we increase τ, we observe a larger increase of the fraction of the population that holds the anti-physical-distancing opinion when $\gamma_{\text{info}} = 2$ than when $\gamma_{\text{info}} = 0.2$.

7. Conclusions and Discussion

We studied the influence of the spread of competing opinions on the spread of a disease. We assumed that pro- and anti-physical-distancing opinions circulate within a population and affect the spread of the disease. We developed a degree-based pair approximation for the time evolution of the expected number of individuals in different compartments and used it to study dynamics on heterogeneous networks with specified inter-layer and intra-layer degree–degree correlations. We examined different approximation schemes for the effective transmission rate of susceptible individuals in the physical layer (on which a disease spreads). We found that the distribution of the opinions of the nodes in a given disease state is correlated both with their own disease states and with the disease states of their neighbors in the physical layer.

Through extensive numerical simulations, we showed that the opinion contagions in our model can either increase or decrease the disease transmission speed, the peak infection counts, and the number of people who become infected. We demonstrated that the overall impact of the opinion dynamics on disease prevalence depends not only on the opinion influence coefficients, but also on the network structure and on how the opinions couple to the spread of the disease.

We found that lengthening the duration (through decreasing the opinion recovery rate) over which people adopt opinions — whether in favor of or against physical

distancing — may help suppress disease transmission. We also saw that physically distancing for too short a duration may still entail a high infection risk; this is well-known for models of infectious diseases with a fully-mixed population.[7,10] We observed that the benefit of a long opinion-adoption period is reinforced when we let the spread of opinions follow SIRS dynamics instead of SIR dynamics. Allowing people to become susceptible to opinions after having a previous opinion helps create neighborhoods in a network's information layer in which adjacent nodes tend to adopt the same opinion over time. Consequently, people who adopt the pro-physical-distancing opinion are more likely to adopt it again later. Although the same phenomenon applies to the spread of the anti-physical-distancing opinion, the difference in the influence of the two opinions on disease transmission rates leads to an asymmetry in their influence on disease prevalence.

Our work examines both beneficial and harmful effects of the spread of opinions on other dynamical processes (such as the spread of a disease). There are many ways to build on our research. Although two competing opinions can have different contagion parameters, we only showed results in which these parameters are identical. One can also study our model when the two competing opinions spread asymmetrically. We also assumed a unidirectional influence from the information layer to the physical layer, but disease states can also influence opinion states,[24,68] and one can incorporate such coupling. Additionally, time-dependent network structures in which node states coevolve with network structures[60,63] are relevant for behavioral changes when individuals adopt opinions about physical distancing. Such time-dependent networks allow one to model changes in contact patterns due to lockdowns and stay-at-home orders. One can also consider additional opinions (e.g. opinions on vaccines) in conjunction with more complex disease dynamics due to vaccines[65] and variants.

Acknowledgments

This research is supported by the NSF's Rapid Response Research (RAPID) Grant DMS-2027438 and by NSF Grants DMS-1922952 and DMS-2027277 through the Algorithms for Threat Detection (ATD) program. It is also supported by Simons Foundation Math + X Investigator Award number 510776. Zheng Lu and Vanessa Lin contributed equally.

References

1. A. Acar, Antecedents and consequences of online social networking behavior: The case of Facebook, *J. Website Promot.* **3** (2008) 62–83.
2. F. B. Agusto, E. Numfor, K. Srinivasan, E. Iboi, A. Fulk, J. M. Saint Onge and A. T. Peterson, Impact of public sentiments on the transmission of COVID-19 across a geographical gradient, preprint (2021), medRxiv 2021.01.29.21250655, doi: https://doi.org/10.1101/2021.01.29.21250655.
3. J. Arino, Describing, modeling and forecasting the spatial and temporal spread of COVID-19 — A short review, preprint (2021), arXiv:2102.02457.

4. F. M. Bass, A new product growth for model consumer durables, *Manag. Sci.* **15** (1969) 215–227.
5. J. Bedson, L. A. Skrip, D. Pedi, S. Abramowitz, S. Carter, M. F. Jalloh, S. Funk, N. Gobat, T. Giles-Vernick, G. Chowell, J. R. de Almeida, R. Elessawi, S. V. Scarpino, R. A. Hammond, S. Briand, J. M. Epstein, L. Hébert-Dufresne and B. M. Althouse, A review and agenda for integrated disease models including social and behavioural factors, *Nature Human Behav.* **5** (2021) 834–846.
6. N. Bellomo, R. Bingham, M. A. Chaplain, G. Dosi, G. Forni, D. A. Knopoff, J. Lowengrub, R. Twarock and M. E. Virgillito, A multiscale model of virus pandemic: Heterogeneous interactive entities in a globally connected world, *Math. Models Methods Appl. Sci.* **30** (2020) 1591–1651.
7. A. L. Bertozzi, E. Franco, G. Mohler, M. B. Short and D. Sledge, The challenges of modeling and forecasting the spread of COVID-19, *Proc. Natl. Acad. Sci. USA* **117** (2020) 16732–16738.
8. L. M. A. Bettencourt, A. Cintrón-Arias, D. I. Kaiser and C. Castillo-Chávez, The power of a good idea: Quantitative modeling of the spread of ideas from epidemiological models, *Physica A* **364** (2006) 513–536.
9. S. Bikhchandani, D. Hirshleifer and I. Welch, A theory of fads, fashion, custom, and cultural change as informational cascades, *J. Political Econ.* **100** (1992) 992–1026.
10. M. C. Bootsma and N. M. Ferguson, The effect of public health measures on the 1918 influenza pandemic in U.S. cities, *Proc. Natl. Acad. Sci. USA* **104** (2007) 7588–7593.
11. F. Brauer, C. Castillo-Chavez and Z. Feng, *Mathematical Models in Epidemiology*, Vol. 32 (Springer-Verlag, 2019).
12. P. Bródka, K. Musial and J. Jankowski, Interacting spreading processes in multilayer networks: A systematic review, *IEEE Access* **8** (2020) 10316–10341.
13. P. C. V. da Silva, F. Velásquez-Rojas, C. Connaughton, F. Vazquez, Y. Moreno and F. A. Rodrigues, Epidemic spreading with awareness and different timescales in multiplex networks, *Phys. Rev. E* **100** (2019) 032313.
14. M. De Domenico, C. Granell, M. A. Porter and A. Arenas, The physics of spreading processes in multilayer networks, *Nature Phys.* **12** (2016) 901–906.
15. O. Diekmann, J. A. P. Heesterbeek and J. A. J. Metz, On the definition and the computation of the basic reproduction ratio R_0 in models for infectious diseases in heterogeneous populations, *J. Math. Biol.* **28** (1990) 365–382.
16. R. Durrett and S. Levin, The importance of being discrete (and spatial), *Theoret. Popul. Biol.* **46** (1994) 363–394.
17. K. T. D. Eames and M. J. Keeling, Modeling dynamic and network heterogeneities in the spread of sexually transmitted diseases, *Proc. Natl. Acad. Sci. USA* **99** (2002) 13330–13335.
18. J. M. Epstein, E. Hatna and J. Crodelle, Coupled contagion: A two-fears epidemic model, *J. Roy. Soc. Interf.* **18** (2021) 20210186.
19. E. Estrada, COVID-19 and SARS-CoV-2. Modeling the present, looking at the future, *Phys. Rep.* **869** (2020) 1–51.
20. D. M. Feehan and A. S. Mahmud, Quantifying population contact patterns in the United States during the COVID-19 pandemic, *Nature Commun.* **12** (2021) 893.
21. B. K. Fosdick, D. B. Larremore, J. Nishimura and J. Ugander, Configuring random graph models with fixed degree sequences, *SIAM Rev.* **60** (2018) 315–355.
22. S. Funk, E. Gilad and V. A. A. Jansen, Endemic disease, awareness, and local behavioral response, *J. Theoret. Biol.* **264** (2010) 501–509.

23. S. Funk, E. Gilad, C. Watkins and V. A. A. Jansen, The spread of awareness and its impact on epidemic outbreaks, *Proc. Natl. Acad. Sci. USA* **106** (2009) 6872–6877.
24. S. Funk, M. Salathé and V. A. A. Jansen, Modeling the influence of human behavior on the spread of infectious diseases: A review, *J. Roy. Soc. Interf.* **7** (2010) 1247–1256.
25. A. Gabbatt, US anti-lockdown rallies could cause surge in COVID-19 cases, experts warn, *Guardian* (2020), https://www.theguardian.com/us-news/2020/apr/20/us-protests-lockdown-coronavirus-cases-surge-warning.
26. R. Gallotti, F. Valle, N. Castaldo, P. Sacco and M. De Domenico, Assessing the risks of 'infodemics' in response to COVID-19 epidemics, *Nature Human Behav.* **4** (2020) 1285–1293.
27. A. Glaubitz and F. Fu, Oscillatory dynamics in the dilemma of social distancing, *Proc. Roy. Soc. A* **476** (2020) 20200686.
28. J. P. Gleeson, High-accuracy approximation of binary-state dynamics on networks, *Phys. Rev. Lett.* **107** (2011) 068701.
29. J. P. Gleeson, Binary-state dynamics on complex networks: Pair approximation and beyond, *Phys. Rev. X* **3** (2013) 021004.
30. W. Goffman and V. Newill, Generalization of epidemic theory, *Nature* **204** (1964) 225–228.
31. C. Granell, S. Gómez and A. Arenas, Dynamical interplay between awareness and epidemic spreading in multiplex networks, *Phys. Rev. Lett.* **111** (2013) 128701.
32. C. Granell, S. Gómez and A. Arenas, Competing spreading processes on multiplex networks: Awareness and epidemics, *Phys. Rev. E* **90** (2014) 012808.
33. Q. Guo, X. Jiang, Y. Lei, M. Li, Y. Ma and Z. Zheng, Two-stage effects of awareness cascade on epidemic spreading in multiplex networks, *Phys. Rev. E* **91** (2015) 012822.
34. Q. Guo, Y. Lei, X. Jiang, Y. Ma, G. Huo and Z. Zheng, Epidemic spreading with activity-driven awareness diffusion on multiplex network, *Chaos* **26** (2016) 043110.
35. N. O. Hodas and K. Lerman, The simple rules of social contagion, *Sci. Rep.* **4** (2014) 4343.
36. N. F. Johnson, N. Velásquez, N. J. Restrepo, R. Leahy, N. Gabriel, S. El Oud, M. Zheng, P. Manrique, S. Wuchty and Y. Lupu, The online competition between pro-and anti-vaccination views, *Nature* **582** (2020) 230–233.
37. M. D. Johnston and B. Pell, A dynamical framework for modeling fear of infection and frustration with social distancing in COVID-19 spread, *Math. Biosci. Eng.* **17** (2020) 7892–7915.
38. B. Karrer and M. E. J. Newman, Competing epidemics on complex networks, *Phys. Rev. E* **84** (2011) 036106.
39. M. J. Keeling, D. A. Rand and A. J. Morris, Correlation models for childhood epidemics, *Proc. Roy. Soc. London Ser. B*: *Biol. Sci.* **264** (1997) 1149–1156.
40. W. O. Kermack and A. G. McKendrick, A contribution to the mathematical theory of epidemics, *Proc. Roy. Soc. London Ser. A Math. Phys. Sci.* **115** (1927) 700–721.
41. I. Z. Kiss, D. M. Green and R. R. Kao, The effect of network mixing patterns on epidemic dynamics and the efficacy of disease contact tracing, *J. Roy. Soc. Interf.* **5** (2008) 791–799.
42. I. Z. Kiss, J. C. Miller and P. L. Simon, *Mathematics of Epidemics on Networks*: *From Exact to Approximate Models*, Vol. 598 (Springer International Publishing, 2017).
43. M. Kivelä, A. Arenas, M. Barthelemy, J. P. Gleeson, Y. Moreno and M. A. Porter, Multilayer networks, *J. Complex Netw.* **2** (2014) 203–271.
44. C. Kuehn, Moment closure — A brief review, *Control of Self-Organizing Nonlinear Systems*, E. Schöll, S. H. L. Klapp, P. Hövel (eds) (Springer International Publishing, 2016), pp. 253–271.

45. S. Lehmann and Y.-Y. Ahn, *Complex Spreading Phenomena in Social Systems*: *Influence and Contagion in Real-World Social Networks* (Springer International Publishing, 2018).
46. J. Lindquist, J. Ma, P. Van den Driessche and F. H. Willeboordse, Effective degree network disease models, *J. Math. Biol.* **62** (2011) 143–164.
47. P. D. Lunn, C. A. Belton, C. Lavin, F. P. McGowan, S. Timmons and D. A. Robertson, Using behavioral science to help fight the coronavirus, *J. Behav. Publ. Administ.* **3** (2020), https://doi.org/10.30636/jbpa.31.147.
48. S. Melnik, M. A. Porter, P. J. Mucha and J. P. Gleeson, Dynamics on modular networks with heterogeneous correlations, *Chaos* **24** (2014) 023106.
49. J. C. Miller, Cocirculation of infectious diseases on networks, *Phys. Rev. E* **87** (2013) 060801.
50. J. C. Miller, A. C. Slim and E. M. Volz, Edge-based compartmental modeling for infectious disease spread, *J. Roy. Soc. Interf.* **9** (2012) 890–906.
51. Y. Moreno, J. B. Gómez and A. F. Pacheco, Epidemic incidence in correlated complex networks, *Phys. Rev. E* **68** (2003) 035103.
52. M. E. J. Newman, Assortative mixing in networks, *Phys. Rev. Lett.* **89** (2002) 208701.
53. M. E. J. Newman, *Networks*, 2nd edn. (Oxford Univ. Press, 2018).
54. M. E. J. Newman and M. Girvan, Mixing patterns and community structure in networks, In: Pastor-Satorras R., Rubi M., Diaz-Guilera A. (eds) Statistical Mechanics of Complex Networks. *Lecture Notes in Physics*, vol 625 (Springer-Verlag, 2003), pp. 66–87.
55. Y. Pan and Z. Yan, The impact of multiple information on coupled awareness–epidemic dynamics in multiplex networks, *Physica A* **491** (2018) 45–54.
56. R. Pastor-Satorras, C. Castellano, P. Van Mieghem and A. Vespignani, Epidemic processes in complex networks, *Rev. Mod. Phys.* **87** (2015) 925–979.
57. K. Peng, Code — A multilayer network model of the coevolution of the spread of a disease and competing opinions (2021), https://gitlab.com/KaiyanP196/coevolution-disease-and-competing-opinions.
58. X.-L. Peng and Y.-D. Zhang, Contagion dynamics on adaptive multiplex networks with awareness-dependent rewiring, *Chin. Phys. B* **30** (2020) 058901.
59. N. Perra, Non-pharmaceutical interventions during the COVID-19 pandemic: A review, *Phys. Rep.* **913** (2021) 1–52.
60. M. A. Porter and J. P. Gleeson, *Dynamical Systems on Networks*: *A Tutorial*, Frontiers in Applied Dynamical Systems: Reviews and Tutorials, Vol. 4 (Springer International Publishing, 2016).
61. X. Qian, J. Xue and S. V. Ukkusuri, Modeling disease spreading with adaptive behavior considering local and global information dissemination, preprint (2020), arXiv:2008.10853.
62. D. N. Rapp and N. A. Salovich, Can't we just disregard fake news? The consequences of exposure to inaccurate information, *Policy Insights Behav. Brain Sci.* **5** (2018) 232–239.
63. H. Sayama, I. Pestov, J. Schmidt, B. J. Bush, C. Wong, J. Yamanoi and T. Gross, Modeling complex systems with adaptive networks, *Comput. Math. Appl.* **65** (2013) 1645–1664.
64. B. She, J. Liu, S. Sundaram and P. E. Paré, On a network SIS epidemic model with cooperative and antagonistic opinion dynamics, preprint (2021), arXiv:2102.12834.
65. M. Stella, M. S. Vitevitch and F. Botta, Cognitive networks identify the content of English and Italian popular posts about COVID-19 vaccines: Anticipation, logistics, conspiracy and loss of trust, preprint (2021), arXiv:2103.15909.

66. F. Velásquez-Rojas, P. C. Ventura, C. Connaughton, Y. Moreno, F. A. Rodrigues and F. Vazquez, Disease and information spreading at different speeds in multiplex networks, *Phys. Rev. E* **102** (2020) 022312.
67. F. Verelst, L. Willem and P. Beutels, Behavioral change models for infectious disease transmission: A systematic review (2010–2015), *J. Roy. Soc. Interf.* **13** (2016) 20160820.
68. Z. Wang, M. A. Andrews, Z.-X. Wu, L. Wang and C. T. Bauch, Coupled disease–behavior dynamics on complex networks: A review, *Phys. Life Rev.* **15** (2015) 1–29.
69. W. Wang, M. Tang, H. Yang, Y. Do, Y.-C. Lai and G. Lee, Asymmetrically interacting spreading dynamics on complex layered networks, *Sci. Rep.* **4** (2014) 5097.
70. Y. Wang, G. Xiao and J. Liu, Dynamics of competing ideas in complex social systems, *New J. Phys.* **14** (2012) 013015.
71. L. Weng, F. Menczer and Y.-Y. Ahn, Virality prediction and community structure in social networks, *Sci. Rep.* **3** (2013) 2522.
72. K.-C. Yang, F. Pierri, P.-M. Hui, D. Axelrod, C. Torres-Lugo, J. Bryden and F. Menczer, The COVID-19 infodemic: Twitter versus Facebook, *Big Data & Society* **8** (2021) 20539517211013861.
73. M. Ye, L. Zino, A. Rizzo and M. Cao, Game-theoretic modeling of collective decision making during epidemics, *Phys. Rev. E* **104** (2021) 024314.
74. Y. Ye, Q. Zhang, Z. Ruan, Z. Cao, Q. Xuan and D. D. Zeng, Effect of heterogeneous risk perception on information diffusion, behavior change, and disease transmission, *Phys. Rev. E* **102** (2020) 042314.
75. J. Zarocostas, How to fight an infodemic, *Lancet* **395** (2020) 676.
76. J. Zhang, M. Litvinova, Y. Liang, Y. Wang, W. Wang, S. Zhao, Q. Wu, S. Merler, C. Viboud, A. Vespignani, M. Ajelli and H. Yu, Changes in contact patterns shape the dynamics of the COVID-19 outbreak in China, *Science* **368** (2020) 1481–1486.